

**KEK 12 GeV Proton Synchrotron**

**Yoshitaka KIMURA**

**National Laboratory for High Energy Physics  
Oho-machi, Tsukuba-gun, Ibaraki-kan, 300-32, Japan**

## I. AIM OF THE TALK

The purpose of this talk is to briefly present the working aspects of the KEK 12 GeV proton synchrotron. We do not explain details of the theories and the instrumentations which are applied to particle acceleration, but try to give sketchy perspectives of accelerators. In the subjects covered by this talk, two important items, vacuum and control systems, are left unexplained. We hope these are taken up in more specialized courses.

## II. GENERALITIES

### (1) General view

The KEK proton synchrotron consists of four stages of accelerators as illustrated in Fig.1. Why did we adopt such a complicated cascade structure, especially the insertion of the booster between the injector and the main ring? We can't answer the question in a word, but may say that a compromise between the construction cost and obtainable beam intensities leads to this solution. However our choice will not be justified until we overcome the difficulties which are inherent to this complication and bring the accelerator to the operation as designed.

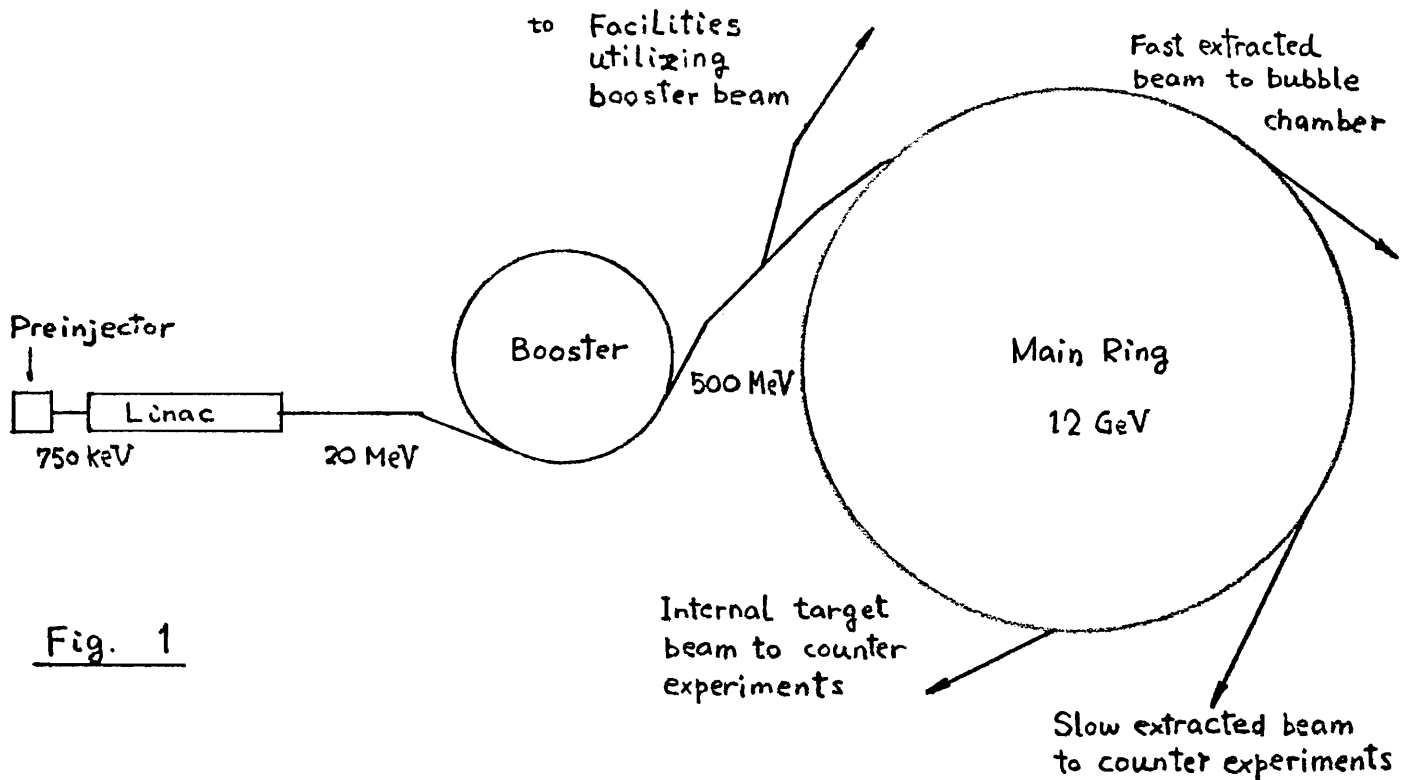


Fig. 1

The construction of the accelerator proceeds as follows.

- Apr. 1971 ; Start of construction.
- Aug. 1974 : Acceleration to 20 MeV in the linac.
- Dec. 1974 : Acceleration to 500 MeV in the booster.
- Mar. 1976 : Acceleration to 10 GeV in the main ring.
- Aug. 1976 : Acceleration of  $1.4 \times 10^{11}$  protons/pulse to 8 GeV.
- Sep. 1976 : Construction of the beam transport tunnel from the booster to facilities which utilize 500 MeV protons.

(2) Accelerator cycles

The pre-injector, linac and booster accelerate 20 beam pulses every second. The main ring has a magnetic field pattern as shown in Fig.2 and starts the acceleration after accepting 9 booster pulses. The booster beams which are not transferred to the main ring will be used for such experiments as neutron diffraction, radiation therapy, and physics of mesic atoms and nucleus, which require high intensity intermediate energy protons. The booster can afford an average proton current of about  $1.5 \mu\text{A}$  ( $\sim 1 \times 10^{13}$  p/sec) to those studies.

(3) Intensity estimation

The nominal beam intensity of the linac is about 100 mA in peak current and 10  $\mu\text{sec}$  in pulse width. The booster is designed in such a way that its acceptance in the horizontal phase space is about five times of the linac emittance. Then, about  $5 \times (0.6 \sim 0.7)$  booster turns of a linac pulse can be injected into the booster, where the factor (0.6 ~ 0.7) is the efficiency of the multi-turn injection. The revolution frequency of 20 MeV proton in the booster is 1.6 MHz and three turns take about 2  $\mu\text{sec}$ . The number of protons stored in the booster at the injection is estimated to be

$$\frac{10^{-1}(\text{A}) \times 2 \cdot 10^{-6}(\text{s})}{1.6 \times 10^{-19}(\text{c})} \approx 1.2 \times 10^{12} .$$

Assuming that a half of this amount is transferred and accelerated in the main ring, we can expect 12 GeV proton intensity of about  $9 \times 1.2 \times 10^{12} \times 0.5 \approx 5 \times 10^{12}$  protons/main ring pulse.

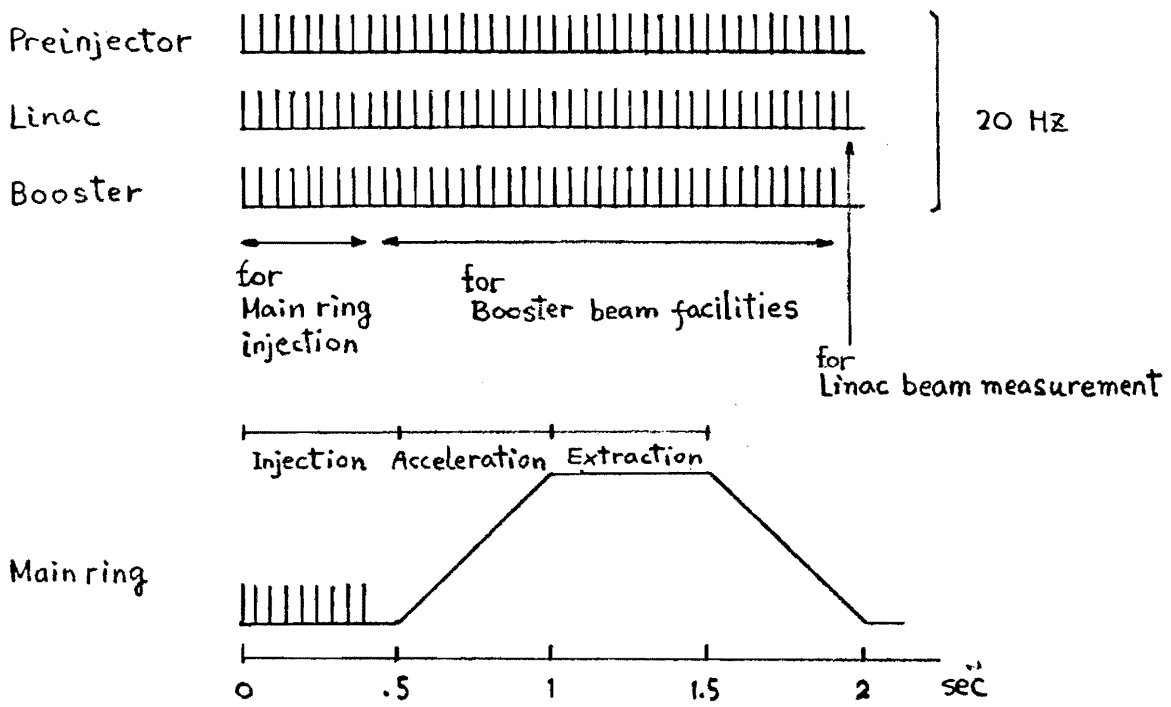


Fig. 2

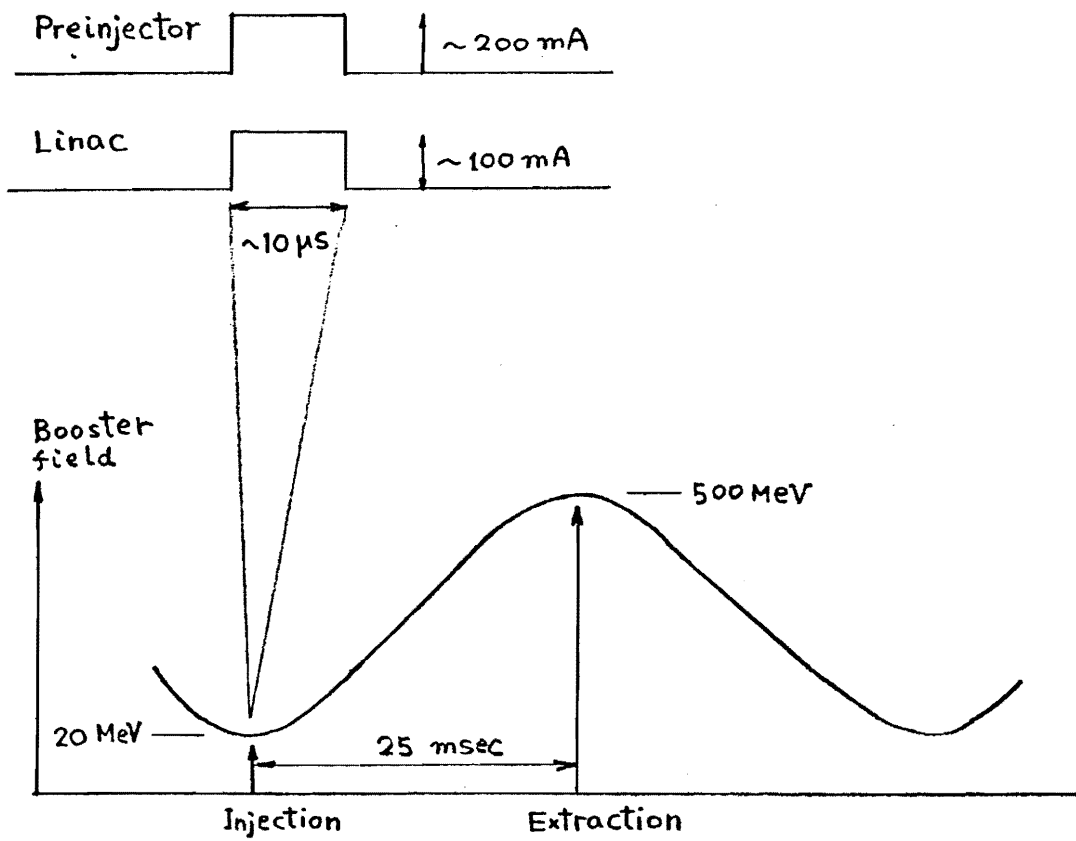


Fig. 3

### III. PRE-INJECTOR

"No Accelerator is better than its injector."

#### (1) System diagram

The pre-injector consists of an open air type Cockcroft-Walton high voltage generator, an ion source, a high voltage terminal which is a power station to operate the ion source, an accelerating column, and a beam transport line between the column and the linac (Fig.4). It must be noted that protons emerging from the ion source are accelerated to 750 keV while traversing a short distance ( $\leq 30$  cm). In an intense beam, effects of defocusing forces due to space charge are appreciable at low energies, so the beam must be accelerated as quickly as possible. The present accelerating column is about 25 cm long and the mean field strength within it reaches about 30 kV/cm.

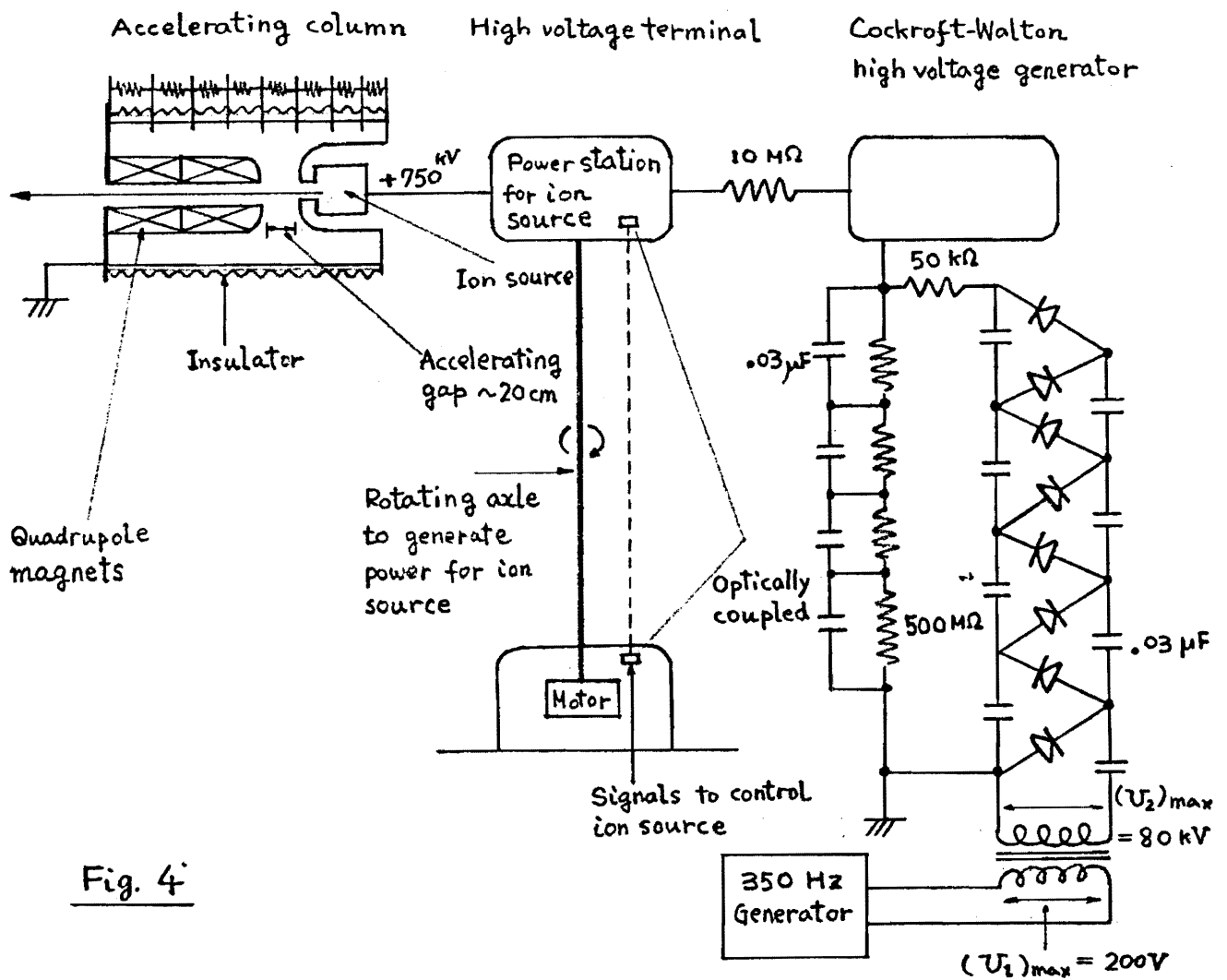
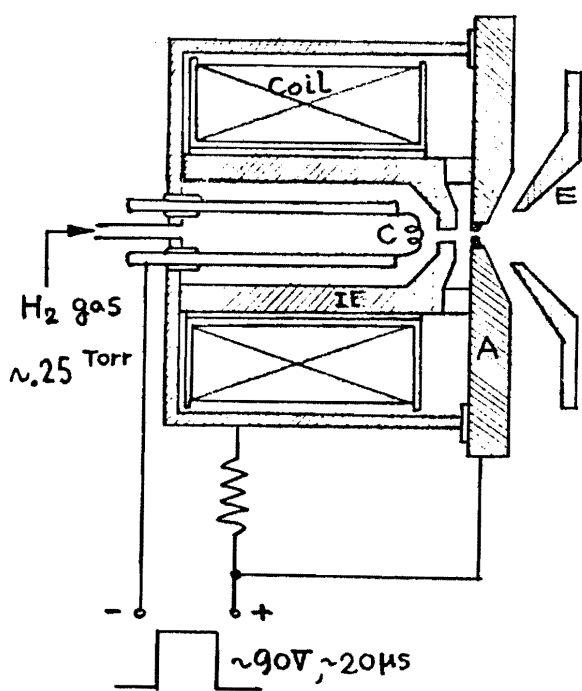


Fig. 4

(2) Ion source

A cross sectional view of the prototype ion source is illustrated in Fig.5. By application of a pulsed potential between the heated cathode and the anode, a low voltage arc discharge operates between them. The discharge is concentrated under electrostatic actions of the intermediate electrode and actions of the intense inhomogeneous magnetic field between the intermediate electrode and the anode. There are two main regions in the source where the arc plasma develops, one is around the cathode (cathode plasma) and the other around the anode (anode plasma). Then, this type of the source is supposedly called "duoplasmatron". Electrons and ions diffuse out from the high density anode plasma through the small anode hole into the expansion region, from which protons are extracted out by a negative extractor electrode.

Figure 6 shows a typical example of the pre-injector current injected into the linac.



- C - Heated cathode
- IE - Intermediate electrode (steel)
- A - Anode (steel)
- E - Extractor electrode (stainless steel)
- - Insulator

Fig. 6

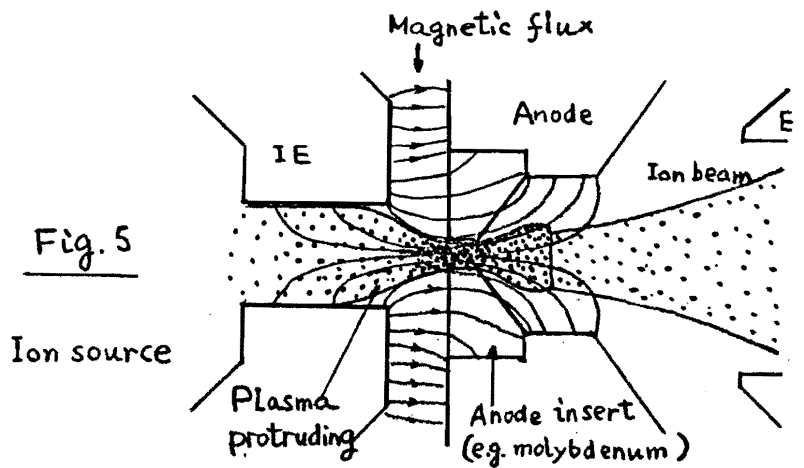
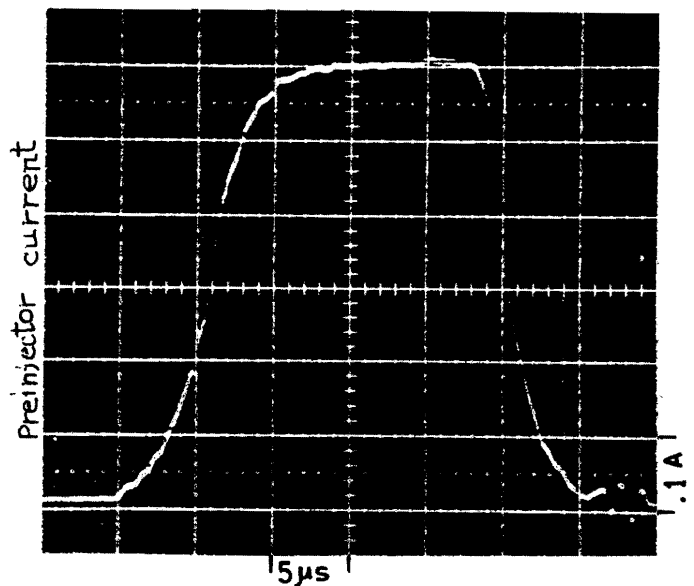


Fig. 5

Ion source



#### IV. LINAC

"The most expensive and the most powerful."

##### (1) Principle of acceleration

An elementary form of the proton linear accelerator (linac) is illustrated in Fig.7. A standing electric field is longitudinally set up in the rf resonator and polarizes the drift tubes. The length of the drift tube ( $L$ ) is so related to the velocity of protons at the tube ( $v$ ) and the rf frequency ( $f = \text{constant}$ ) that protons coast within the tube, field free region, when the gap field between the drift tubes points wrong direction and traverse the gap when the field points right direction;  $L = v/f$ . The present linac is operated at 200 MHz. There are 89 accelerating gaps (90 drift tubes) and the peak accelerating field strength is about 9 MV/m.

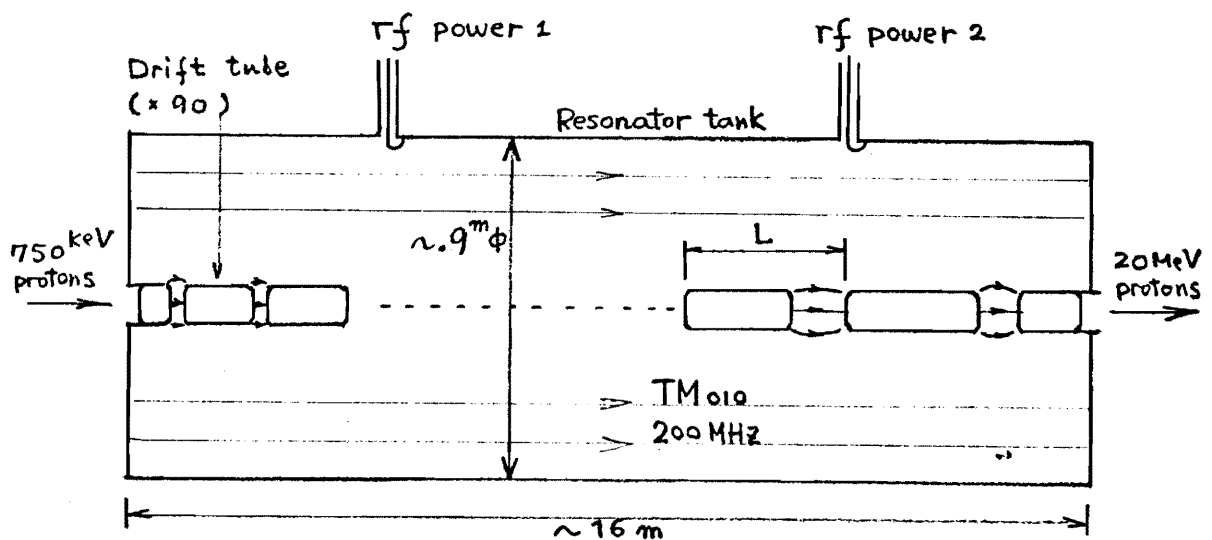


Fig.7

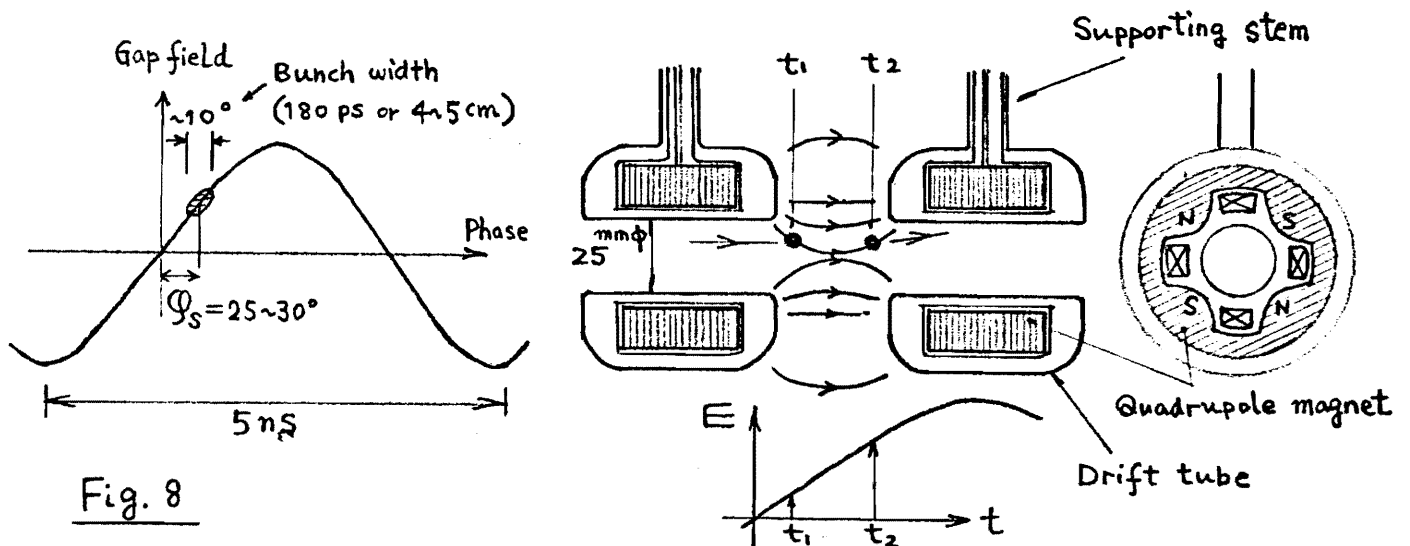


Fig. 8

(2) Transverse focusing by quadrupole magnets

As is well-known, particles are accelerated stably for the longitudinal motion, if they occupy a phase region centered about the synchronous phase ( $\phi_s$ ) which is on the rising side of the voltage across the gap. But this requirement for phase stability causes lateral defocusing effects on off-axis particles within the gap as shown in Fig.8. Off-axis particles experience converging forces as they enter the gap and diverging forces as they leave. Since the electric field increases with time in the stable phase region, the diverging force dominates the converging one integrated over the transit time of particles in the gap. To compensate for this effect, quadrupole magnets are used as focusing devices. The quadrupoles are mounted inside the drift tubes and excited in such polarities that converging and diverging forces alternately act on particles which traverse the drift tubes successively.

A quadrupole magnet has the pole face arrangement and the field as illustrated in Fig.9. It exerts forces on the beam which are convergent in one transverse plane and divergent in the other. Particles will show such a trajectory projected on one transverse plane as indicated in Fig.10 within an alternating sequence of quadrupoles, where the quadrupole is represented as a convergent or divergent optical lens. It is noticeable in the figure that the distance of the trajectory from the axis is greater in the convergent unit than in the divergent one, provided quadrupoles are so spaced that the trajectory does not cross the axis. The force acting on a beam in the quadrupole is proportional to its distance from the axis, so the overall function of the alternating sequence of quadrupoles turns out to be convergent.

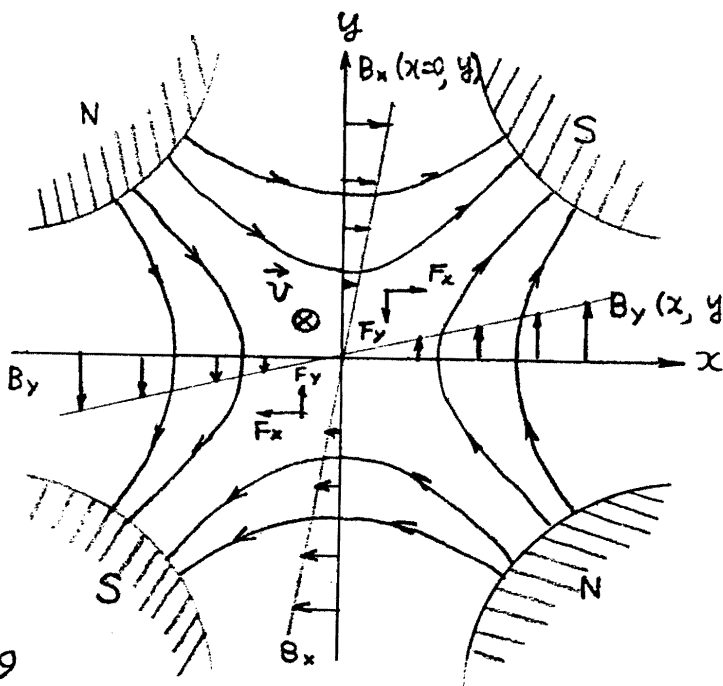


Fig. 9

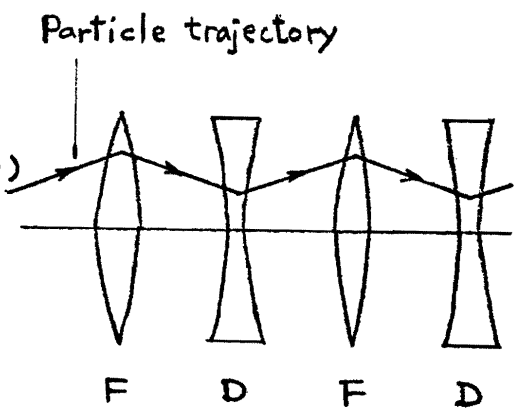


Fig. 10

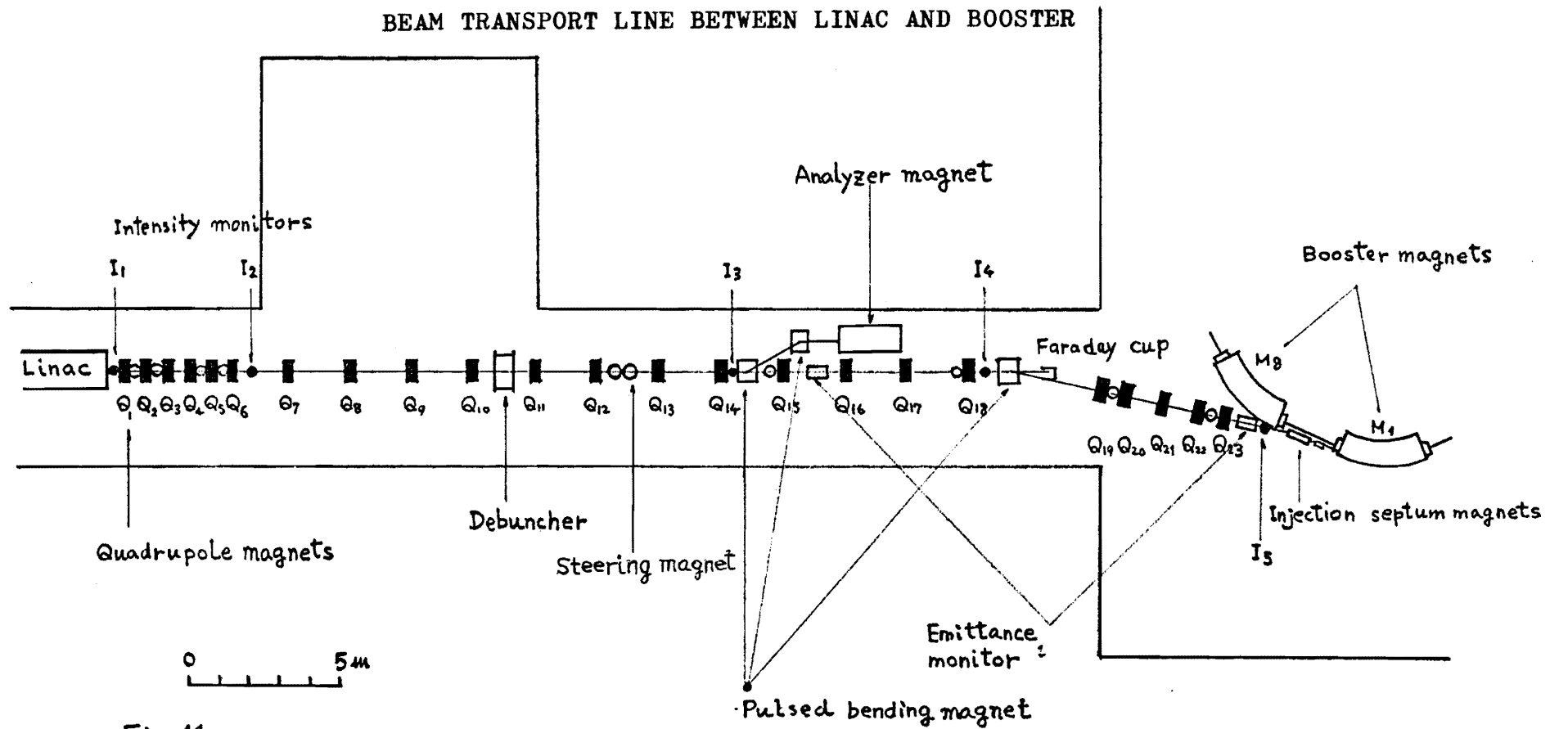


Fig. 11

(3) Beam transport between the linac and the booster

Particles emerging from the linac are transported to the booster through an array of quadrupole magnets as shown in Fig.11. Within the transport line, the transverse emittance of the beam is transformed to what matches with the booster acceptance, and the momentum spread is reduced by use of an extra short rf cavity (so called debuncher) whose rf field is properly phased with that of the main linac cavity. We measure the intensity (Fig.12), the momentum spread (Fig.13), the profiles, and the emittance (Fig.14) of the linac beam in the line.

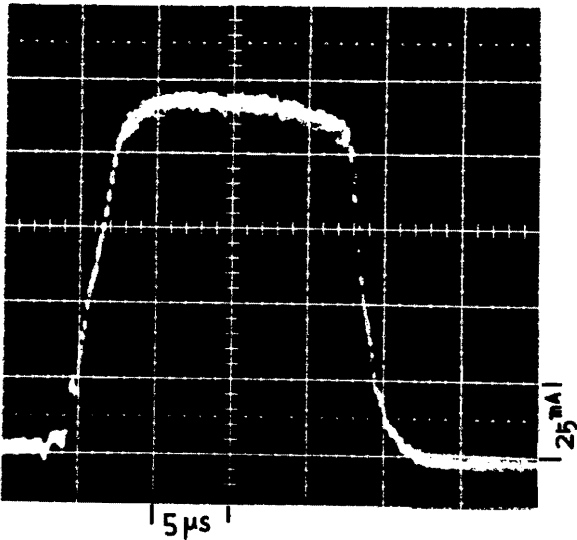


Fig.12 Linac beam intensity

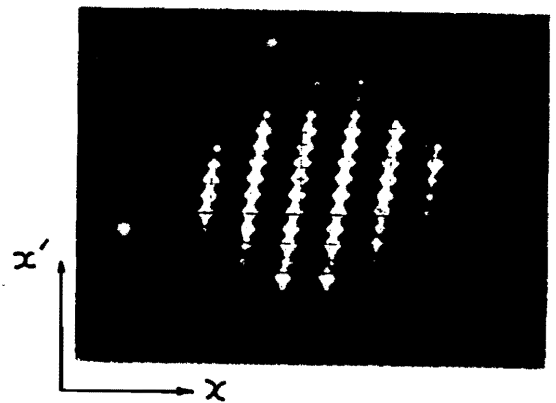


Fig.14 Linac beam emittance  
( $E \sim 40\pi$  mm.mr)

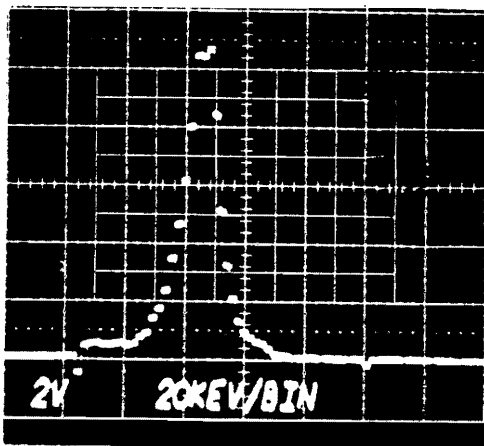
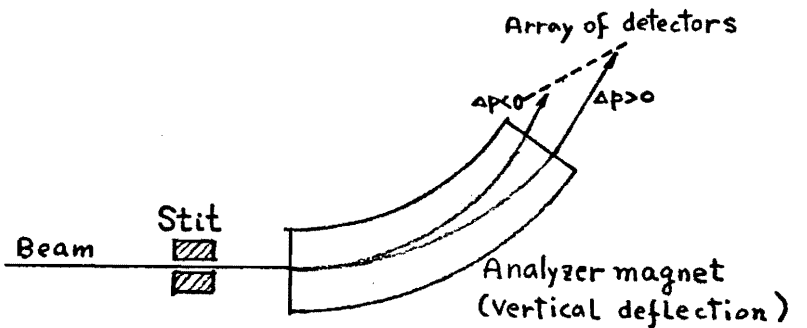


Fig.13 Linac beam energy spread



V. BOOSTER

"Piquant though small."

(1) Magnet system

Figure 15 shows a plan view of the booster magnet and assembly. The ring is composed of eight magnet sectors and field free regions (straight sections) which are essential to accommodate a rf cavity and various kinds of beam handling equipments.

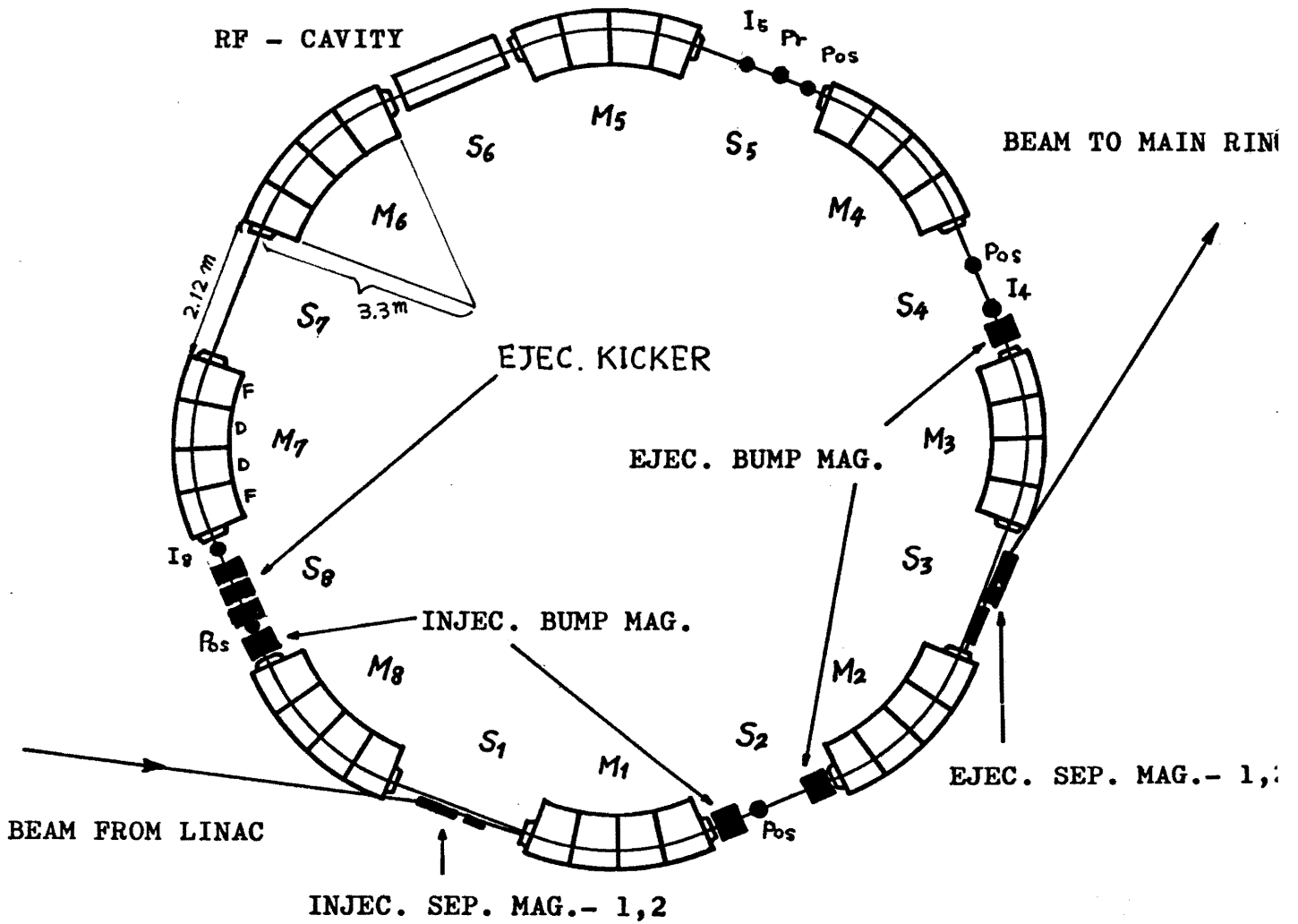


Fig. 15 Booster ring

The magnet is a combined function type and has a cross-section as illustrated in Fig.16. The pole faces are so shaped that the field in the gap is a superposition of a dipole component for the function of bending and a quadrupole component for the function of transverse focusing. There are two types of the magnet unit, F type and D type, which generate the field gradient directed radially inward and radially outward, respectively. The F(D) has a quadrupole field which is convergent (divergent) in the horizontal plane and divergent (convergent) in the vertical plane. As mentioned previously, the alternating sequence of F and D results in convergence for both radial and vertical displacements of particles. Within such a magnet structure, particles perform oscillations about an equilibrium orbit (so called betatron oscillation). In the case of the booster, the frequencies of the betatron oscillation in horizontal and vertical coordinate are  $\nu_H \approx 2.1$  and  $\nu_V \approx 2.2$  in unit of the revolution frequency. The mean radius of the booster (circumferential length divided by  $2\pi$ ) is 6 m, and the bending radius of the magnet is 3.3 m. Figure 17 shows the excitation pattern of the magnet. A field strength

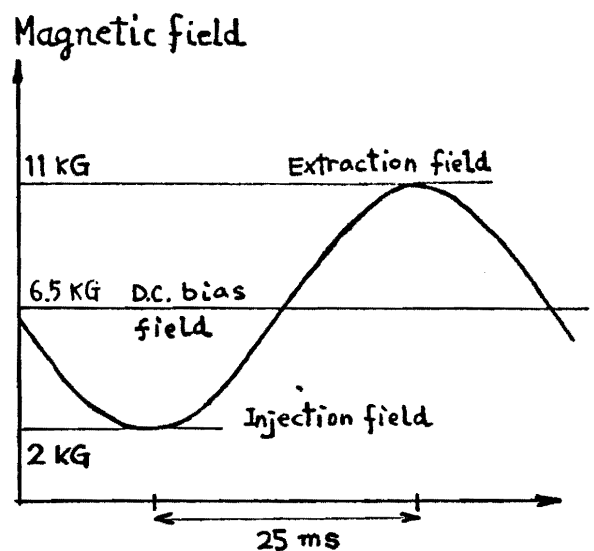
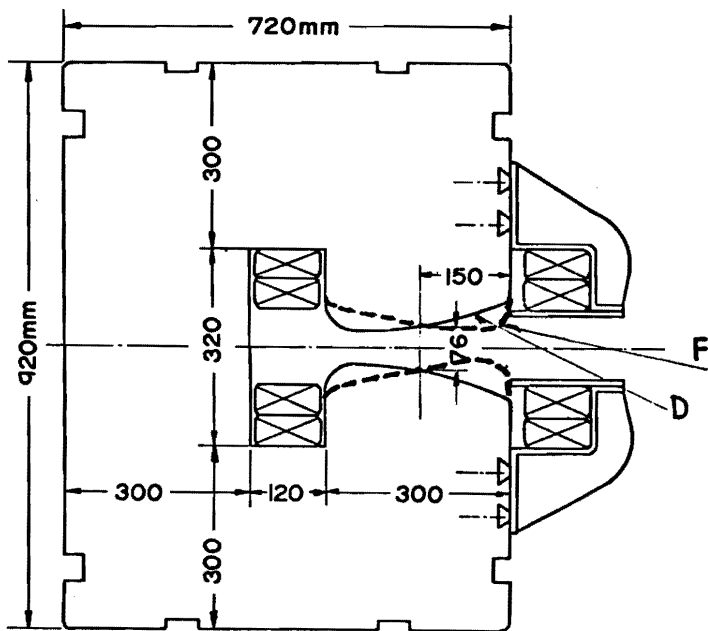


Fig.17

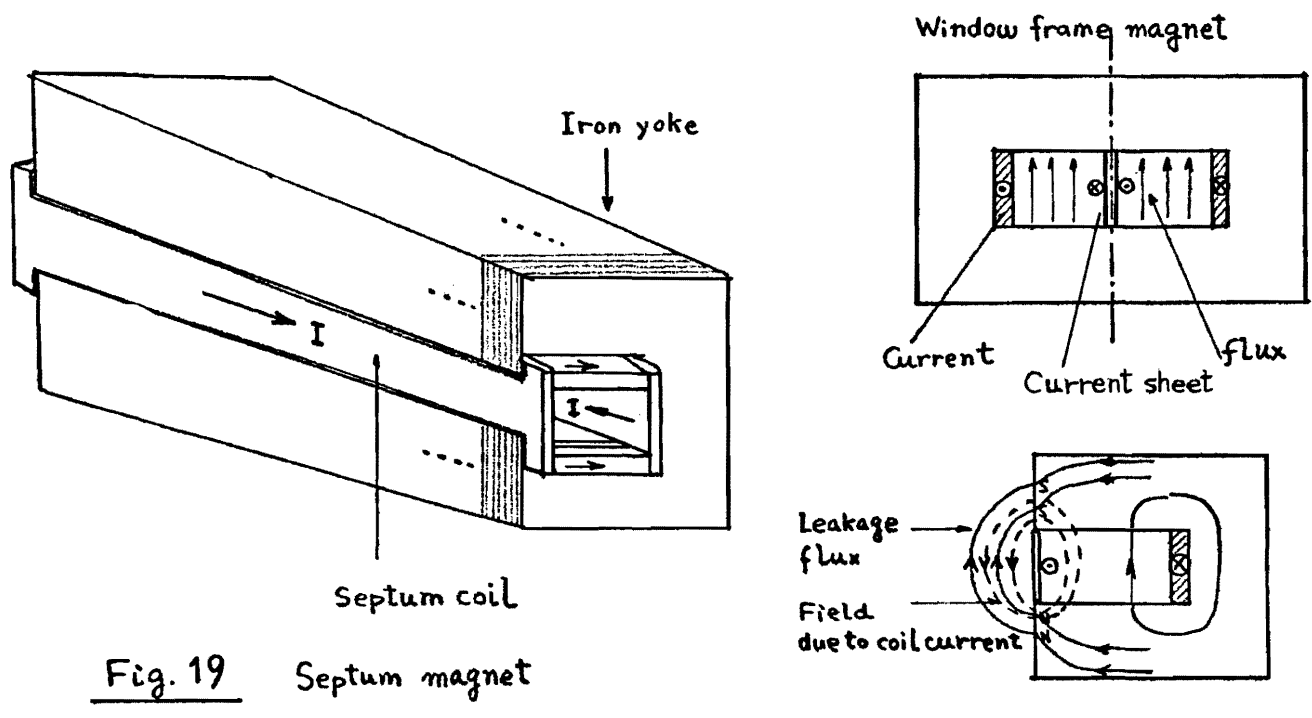
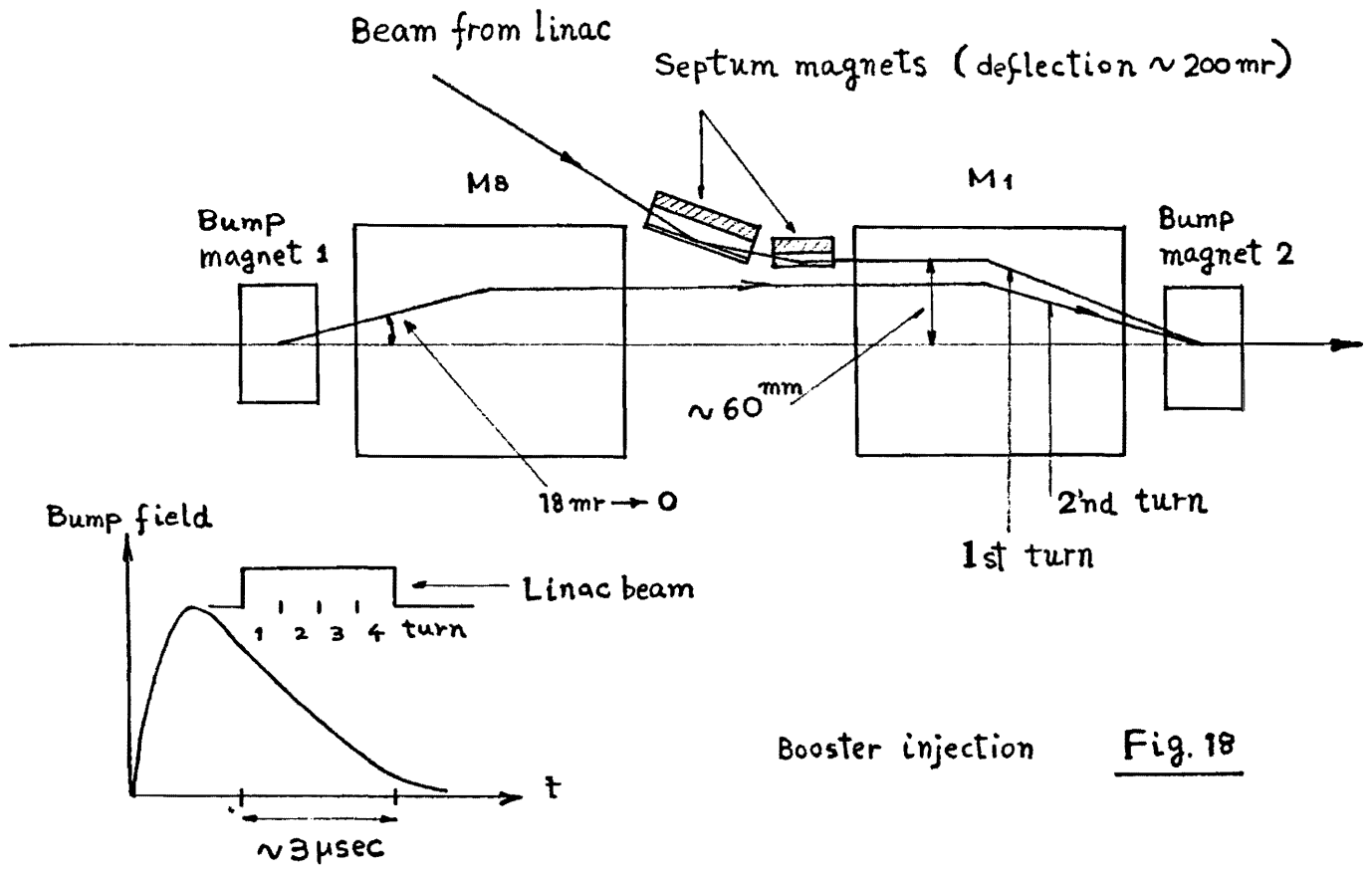
Fig.16 Cross section of booster magnet

(B) is related to beam momentum ( $p$ ) and bending radius ( $\rho$ ) as  $p = eB\rho$  or  $p(\text{GeV}/c) = 0.3 B(\text{T}) \times \rho(\text{m})$  for proton. The magnet core is fabricated by stacking thin insulated iron plates (0.35 mm thick) to reduce a field, which is generated by eddy currents induced in the core, to a tolerable level. Eddy currents induced in the metallic doughnut also cause serious effects for the magnetic field in the gap. To avoid this, the present booster employs special corrugated stainless-steel vacuum tubes which effectively have high electric resistance for unit length, which is equivalent to that of 0.03 mm thick straight stainless pipe.

## (2) Multi-turn injection

Two septum magnets located in the straight section  $S_1$  put the beam from the linac on an orbit which is separated from the central axis by  $\sim 6$  cm and parallel to an equilibrium orbit in  $S_1$  (Fig.18). The equilibrium orbit at the injection has a bump at  $S_1$  and is formed by a pair of pulsed bending magnets (bump magnet) which are located at downstream end of  $S_8$  and at upstream end of  $S_2$ . By decreasing the distance between the bumped and the central orbit at  $S_1$  from  $\sim 6$  cm to 0 during the injection process, we can stack the beam streaming in through the septum magnets turn by turn in the horizontal acceptance of the booster.

The septum magnet has a structure as schematically shown in Fig.19. The special of this magnet is that a strong dipole field is produced inside a thin septum coil, while a quite weak (essentially zero) field outside. The septum magnet is considered to be a half of the window-frame magnet cut along the vertical plane of symmetry, in which a current sheet is inserted to keep the boundary condition that no transverse field component on the symmetry plane. In actual magnets, there remains a field outside the septum due to leakage flux from the core surfaces and field produced by the current septum, though these tend to cancel out each other outside the septum. For example, the upstream septum for the booster injection has septum thickness = 5 mm, field inside the septum = 2 KG, and field outside  $\approx 10$  G at  $\sim 2$  mm from the septum. By covering the outside surface of the septum coil with a thin iron sheet, the external field can be reduced further.



(3) Radio frequency acceleration system

The harmonic number (number of beam bunches in the ring) of the booster is chosen to be one. The accelerating frequency coincides with the revolution frequency. The frequency varies from 1.6 MHz at injection (20 MeV) to 6 MHz at extraction (500 MeV). The accelerating potential applied across the accelerating gap is determined both by an energy increment required for matching the beam momentum to the increasing magnetic field and by a potential which provides the beam with the prescribed momentum spread with a sufficiently large phase space area for stable phase oscillations (so called rf bucket). The booster requires a peak acceleration voltage of about 20 kV.

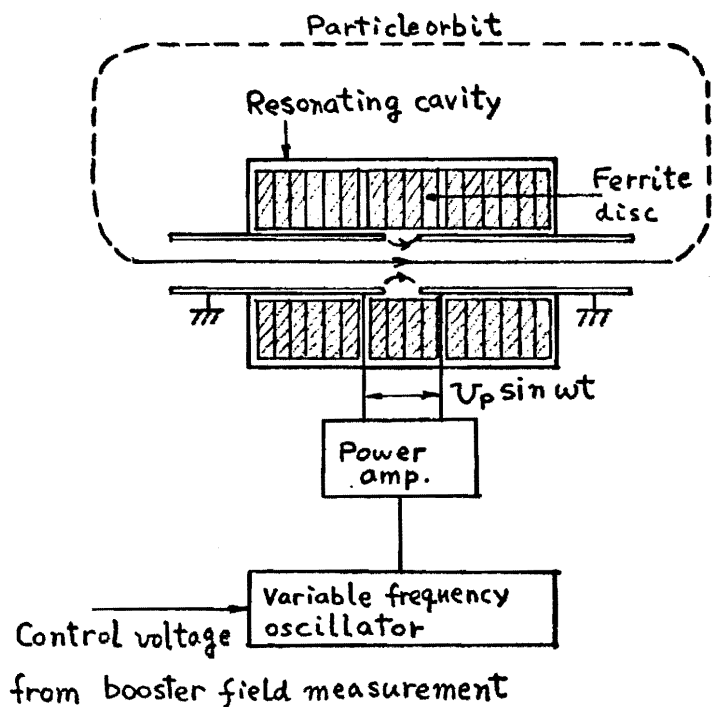
Such an accelerating field is produced across a short insulated gap inside a resonating cavity, which is filled with ferromagnetic material (ferrite) to tune its resonance frequency to that required for the acceleration (Fig.20). Crossing the gap, particles which traverse within the grounded metal tube for most of their path in the ring experience an electromotive force which is induced by a change of magnetic flux linking the orbit in the cavity. This induced voltage eventually coincides with the voltage applied across the gap by the power supply. The resonance frequency of the cavity is swept over the required frequency range (1.6 - 6 MHz) by controlling the permeability of the ferrite which is brought to a partially saturating level by means of the external biasing magnetic field.

$$\text{rot } \vec{E} = - \frac{\partial \vec{B}}{\partial t}$$

$$\oint_{\text{orbit}} \vec{E} \cdot d\vec{l} = - \int_S \left( \frac{\partial \vec{B}}{\partial t} \right) \cdot \vec{n} dS$$

rate of flux change  
in the cavity  
= accelerating  
potential

Fig. 20



To accelerate the beam keeping deviations of the orbit from the central orbit small enough, the accelerating rf frequency should be regulated accurately running after the instantaneous level of the guiding magnetic field, for example a tolerable frequency error is  $|\frac{\Delta f}{f}| \lesssim 3 \times 10^{-4}$  for a deviation of 1 mm at 500 MeV. In the present rf system, the frequency is generated with a variable frequency oscillator which is controlled by the voltage corresponding to the magnetic field measured instantaneously.

(4) Measurement of beam intensity and position

A beam intensity is measured by use of a current transformer which has only a secondary winding on an annular ferrite or permalloy core. The beam which traverses inside of the core forms a primary current of the transformer (Fig.21). The output of the secondary coil passes to

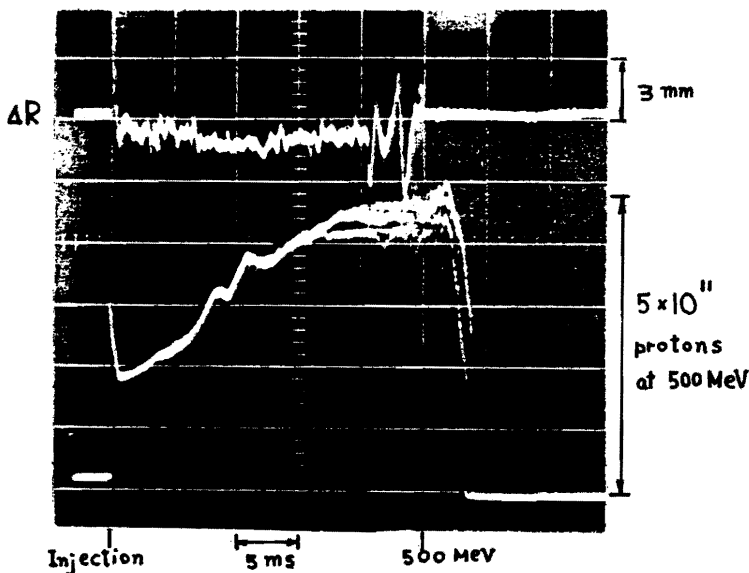


Fig.22 Booster beam intensity

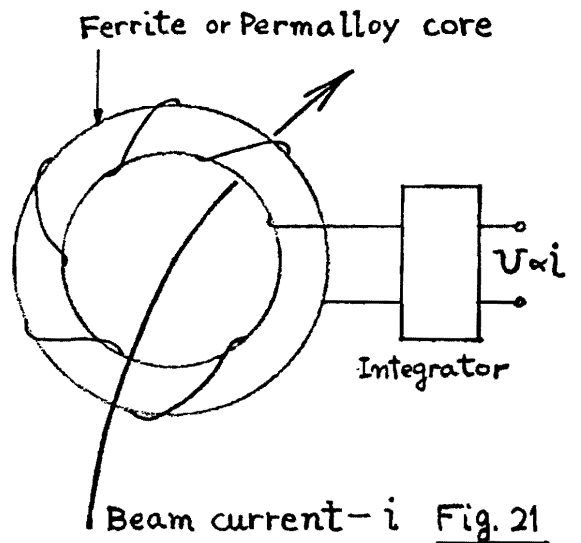


Fig. 21

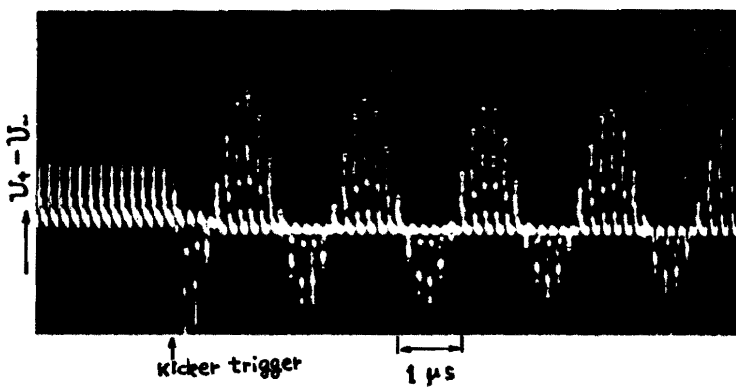


Fig.24 Coherent betatron oscillation in the booster

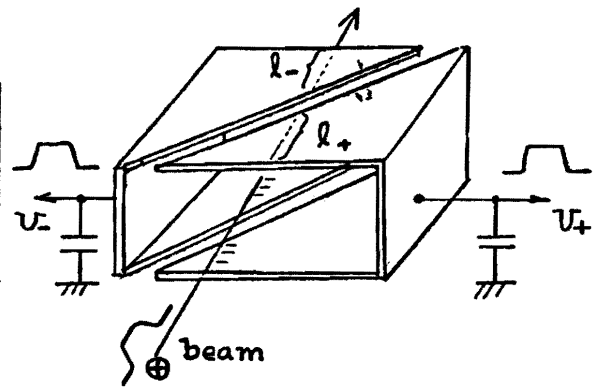


Fig. 23

$$\begin{aligned}
 U_+ &= k l_+ \\
 U_- &= k l_- \\
 \Delta R &\propto \frac{l_+ - l_-}{l_+ + l_-} = \frac{U_+ - U_-}{U_+ + U_-}
 \end{aligned}$$

a sort of integrating circuit working in a short circuited mode and gives an output voltage which proportional to the beam intensity. Figure 22 shows an evolution of the booster intensity in the course of the acceleration. The current decreases by about 30 % till 1 ms after the injection indicating a beam loss during the initial capture process, and starts increasing after that corresponding to the increasing velocity of particles.

We measure radial (vertical) beam positions with a pick-up electrode as schematically shown in Fig.23. The electrode is a short conductor pipe with a rectangular cross section, which is divided into two triangular parts sharing the diagonal. A beam pulse traversing the electrode induces charges on the conductor surfaces. The amount of the induced charges is proportional to the path length of the beam in the electrode, and the charges on the electrode with the triangular area is related to the radial (vertical) beam position. If the output voltages from the pair of the triangular electrodes (Fig.23) are  $v_+$  and  $v_-$ ,  $(v_+ + v_-)$  gives a measure of the beam intensity and  $(v_+ - v_-)/(v_+ + v_-)$  gives a measure of the radial (vertical) beam position. Figure 24 shows an example of  $(v_+ - v_-)$  when a coherent horizontal betatron oscillation is excited in the booster by giving a fast kick to the beam.

#### (5) Extraction

The beam extraction from the booster is schematically explained in Fig.25. As the booster field reaches the top, two bump magnets, one is located at downstream end of S2 and the other upstream end of S4, deform the orbit in such a way that the beam traverses just outside of the coil of the septum magnets in S3 without grazing it. At the instant when the beam should be extracted, three modules of the fast kicker magnet located in S8 give a quick deflection to the beam, which induces a betatron oscillation around the bumped orbit. The oscillation has the maximum amplitude at the septum, and, if the kick is strong enough, the beam jumps into the septum magnet and is fully extracted.

The kicker is a special type of a pulsed bending magnet with fast rise time, whose field starts rising after the tail of the beam bunch passes the kicker and should reach the flat top before the bunch head takes a turn round the ring. In the case of the booster extraction, the kicker rise time should be shorter than 80 nsec including the travelling

time of the pulsed field through the kicker.

The present kicker is a sort of the lumped parameter delay line (Fig.26). The inductance is determined by the magnet aperture where the magnetic field is concentrated with C shaped ferrite cores, and the capacitance is formed by pairs of wide fin plates attached to the ground and high voltage electrode. The kicker is required to have the pulse rise time faster than 30 nsec, so the passband of this delay line magnet should extend over frequencies higher than ~30 MHz. This is achieved by making the length of a unit cell short enough, and using ferrite cores which have large permeability at such frequencies.

A module of the present kicker has length = 32 cm, number of unit cells = 12, inductance = 3.5  $\mu\text{H}/\text{m}$ , capacitance = 2.9 nF/m, characteristic impedance = 25  $\Omega$ , and travelling time of the pulse = 40 ns. Three kicker modules used for the booster extraction generate a field of 450 G. The current to drive the kicker is a pulse of 1.6 kA - 40 kV and is obtained by switching a deuterium filled thyratron. Figure 27 shows a bunch in the booster just before the extraction and that extracted to the transport line between the booster and the main ring together with a current pulse of the kicker.

#### (6) Beam transport between the booster and the main ring

This transport line links the booster to the main ring separated by about 50 m. Since these two accelerators have quite different focusing structures, one of the main roles of the line is to transform the shape of the extracted beam from the booster to what is acceptable in the main ring. This tuning of transverse emittances is performed with an array of quadrupoles and monitors to measure beam profiles at various positions in the line (Fig.28).

The profile monitor is a secondary electron emission type. The principle underlying it is that protons incident upon a conductor eject secondary electrons and the conductor acquires positive charges, provided it is insulated. A high energy proton, say 500 MeV, incident on an aluminum foil will eject electrons with a probability of about a few percent. The output voltage produced at the capacity of the foil is proportional to the number of protons which traverse the foil. The profile monitor consists of several of such a thin aluminum strip or a tungsten wire, which are mounted on a ceramic frame with a separation of a few mm. Examples of the beam profiles measured in the line are shown in Fig.28.

SINGLE BUNCH EXTRACTION FROM THE BOOSTER

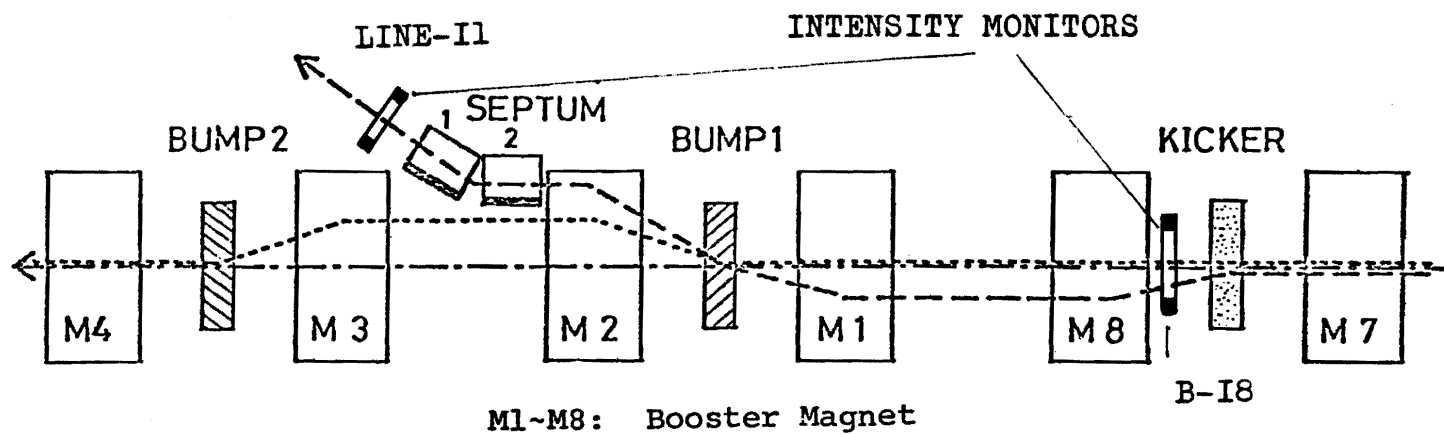
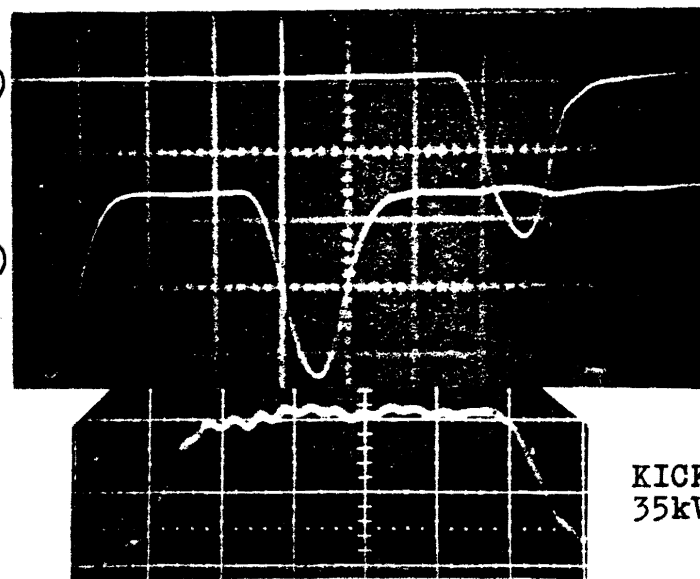


Fig.25

- 156 -

BUNCH IN THE LINE ( I1 )

BUNCH IN THE BOOSTER( I8 )



KICKER MAGNET CURRENT  
35kV - 1.4kA

Fig.27

50 nsec/div

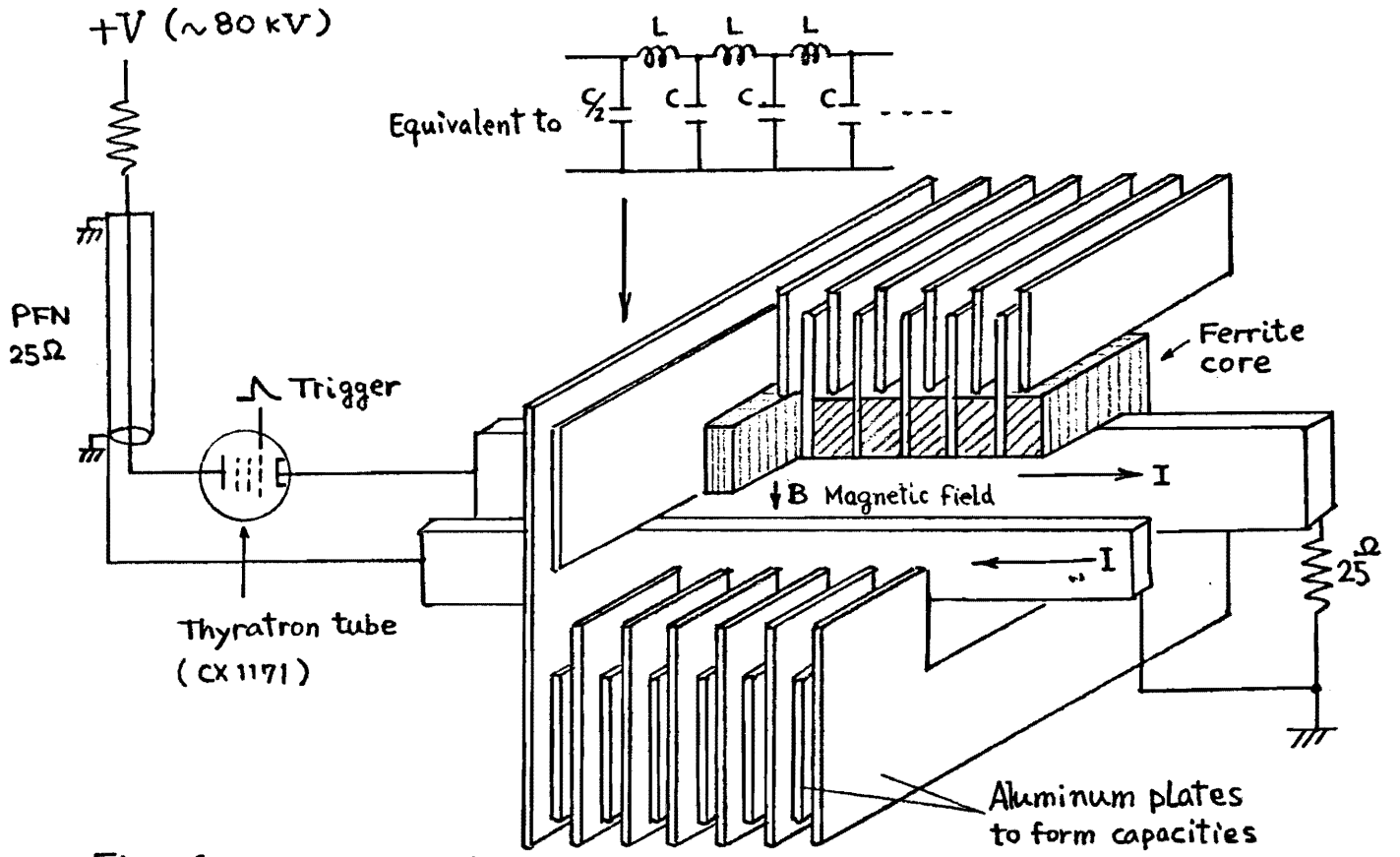
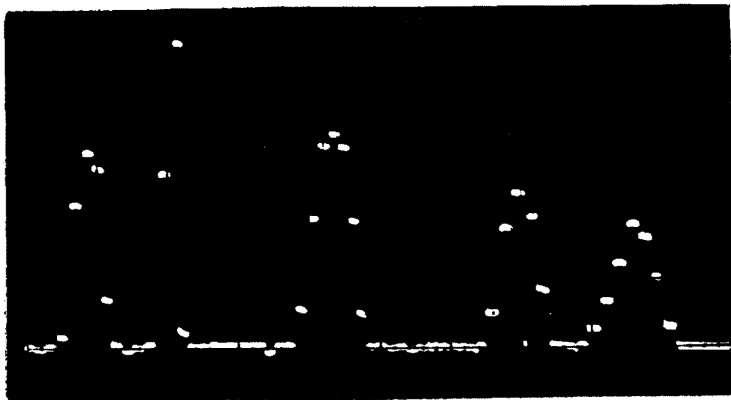


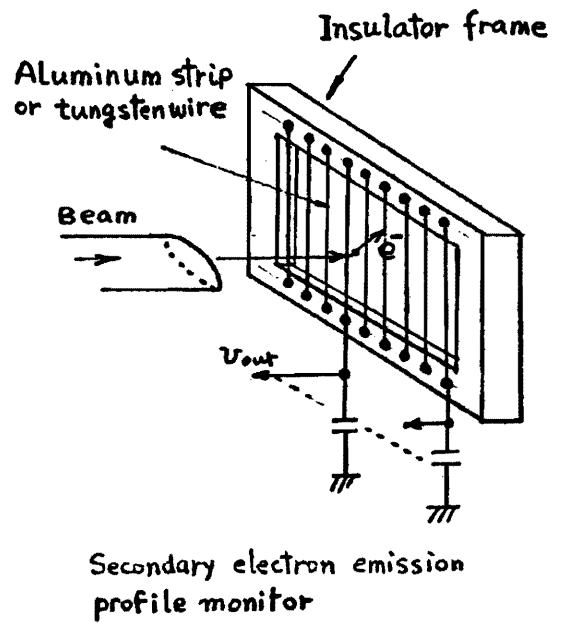
Fig. 26 Kicker magnet



Pr1 H-V      Pr2 H      Pr3 H-V  
 8 mm/bin    4 mm/bin    4 mm/bin

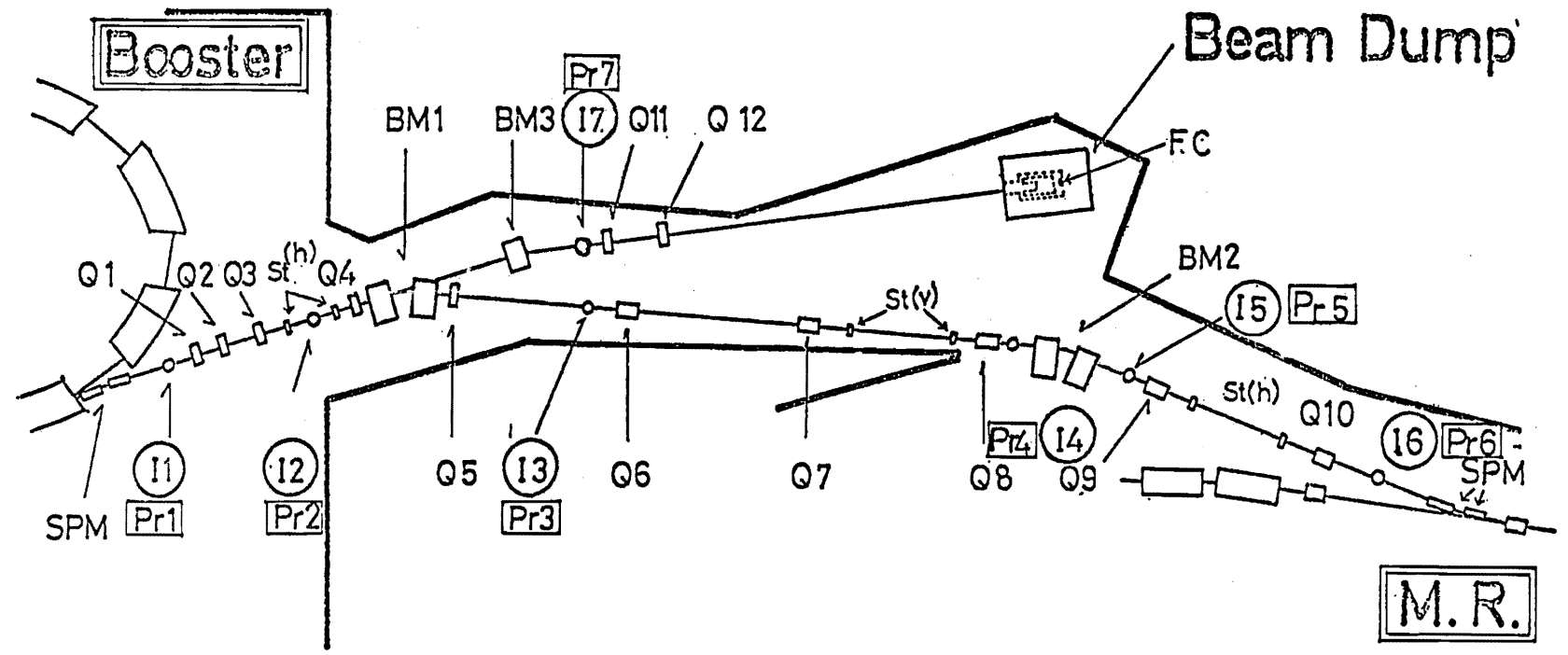
BEAM PROFILES IN THE TRANSPORT LINE

Fig. 28



BEAM TRANSPORT BETWEEN THE BOOSTER AND THE MAIN RING

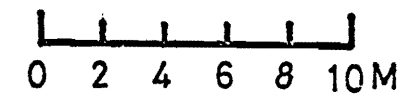
- 158 -



SPM: Septum Magnet  
 Q1 ~ Q12: Quadrupole Magnet  
 BM1-BM3: Bending Magnet  
 St: Steering Magnet

I1 ~ I7: Intensity Monitor  
 Pr1-Pr7: Profile Monitor

Fig. 28



## VI. MAIN RING

"The biggest, but the most delicate."

### (1) Magnet system

Figure 29 shows a plan view of the main ring. The main ring is a separated function type synchrotron, which separately has dipole magnets for the function of bending and quadrupole magnets for the function of focusing. This has an advantage over the combined type in a respect that the focusing conditions (betatron oscillation frequencies) are adjustable. The magnet lattice of the ring is composed of 28 unit cells (12.12 m long), which are separated into four equivalent groups, so called superperiod. There are two types of the unit cell, N and L as illustrated in Fig.30. The L section is the N section missing one dipole unit to provide a long straight section for accommodation of rf cavities or beam handling equipments for injection and extraction. One superperiod is the array of the unit cells as  $(L_1L_2N_3N_4N_5N_6N_7)$ .

The mean radius of the ring is 54 m and the bending radius in the dipole is 24.6 m. It must be noted that the main ring radius is chosen to be nine times of the booster radius so that the main ring is just filled up with nine booster pulses. The operating cycle of the magnetic field is shown in Fig.31. The betatron frequencies of the main ring are normally set at  $\nu_H \approx 7.15$  and  $\nu_V \approx 7.2$  in unit of the revolution frequency.

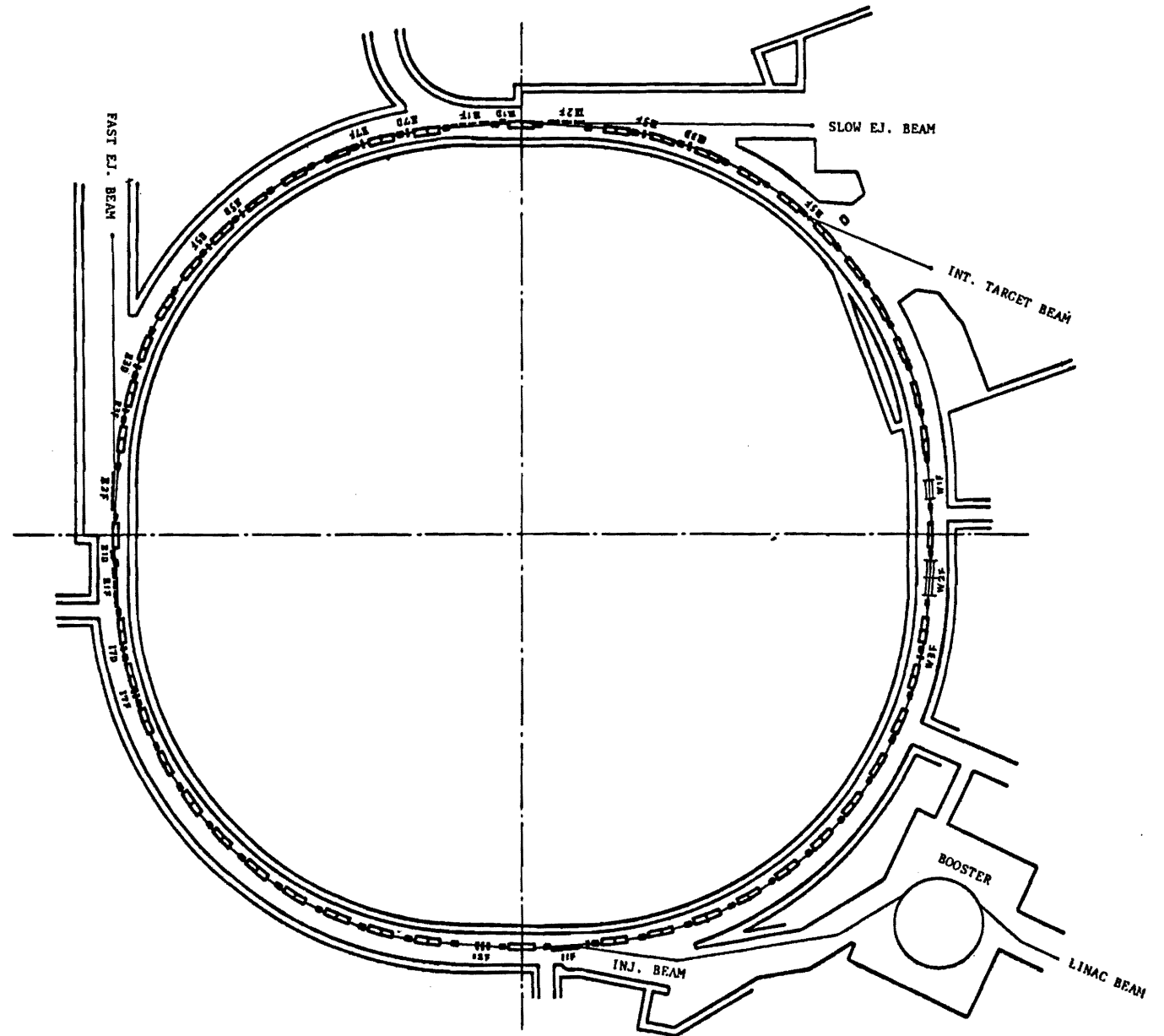
Figure 32 shows cross sections of the main ring dipole and quadrupole magnet. The magnet core is fabricated by stacking 1 mm thick iron plates. The acceleration cycle of the main ring is so slow that even slight imperfections in the magnetic field causes deteriorations of the beam quality. Therefore, in addition to the careful fabrication of the each magnet unit, special attentions should be paid to the alignment of these magnets along the ring. The present magnets are positioned with an accuracy better than  $\pm 0.1$  mm in the position and  $\pm 0.2$  mr in the tilt.

Currents to generate the required field in a dipole or quadrupole magnet with iron yoke can approximately be estimated as illustrated in Fig.33.

- I1F Q MAG. for SLOW EJ.
- I1F SEPTUM MAG. for INJ.
- I2F KICKER for INJ.
- I7F BUMP for FAST EJ.
- I7F FAST BUMP for FAST EJ.
- I7D BUMP for FAST EJ.
- II1F E.S. SEPTUM for FAST EJ.
- II1F SEPTUM MAG. for FAST EJ.
- II1D SEPTUM MAG. for FAST EJ.
- II2F EXT. MAG. for FAST EJ.
- II3F BUMP for FAST EJ.
- II3D BUMP for FAST EJ.
- II5F OCT. MAG. for SLOW EJ.
- II5D FAST BUMP for FAST EJ.
- II7F BUMP for SLOW EJ.
- II7D BUMP for SLOW EJ.
- III1F E.S. SEPTUM for SLOW EJ.
- III1F SEPTUM MAG. for SLOW EJ.
- III1D SEPTUM MAG. for SLOW EJ.
- III2F EXT. MAG. for SLOW EJ.
- III3F BUMP for SLOW EJ.
- III3D BUMP for SLOW EJ.
- III5F INTERNAL TARGET
- IV1F RF CAVITY
- IV2F RF CAVITY
- IV3F Q MAG. for SLOW EJ.

KEK 12 GeV MAIN RING

Fig. 29



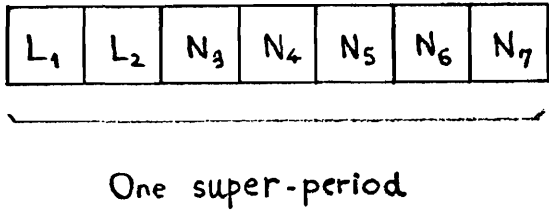
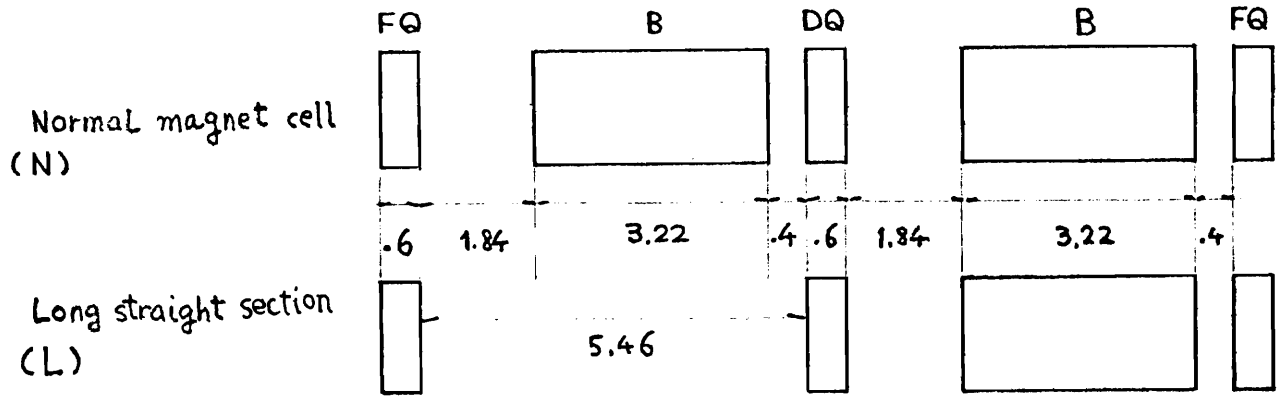


Fig. 30

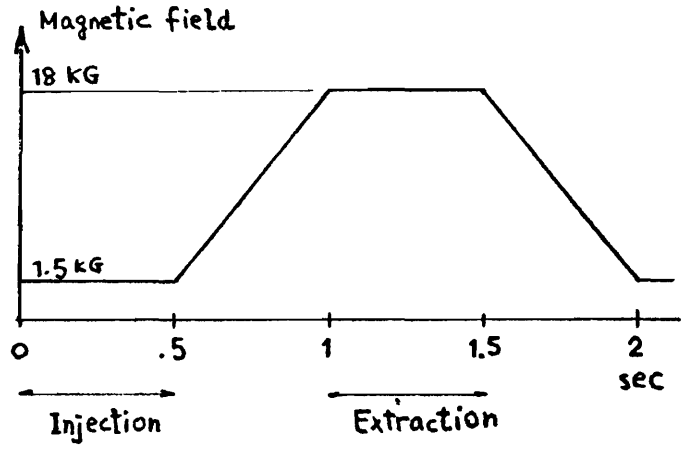


Fig. 31

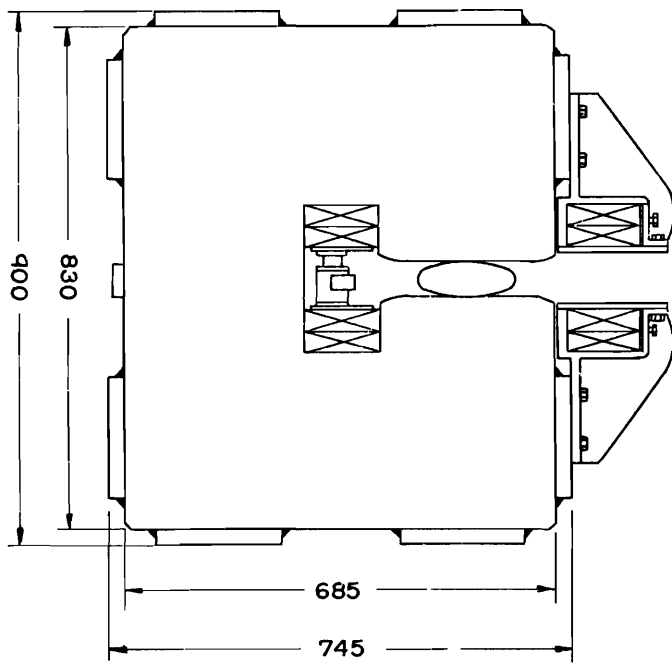
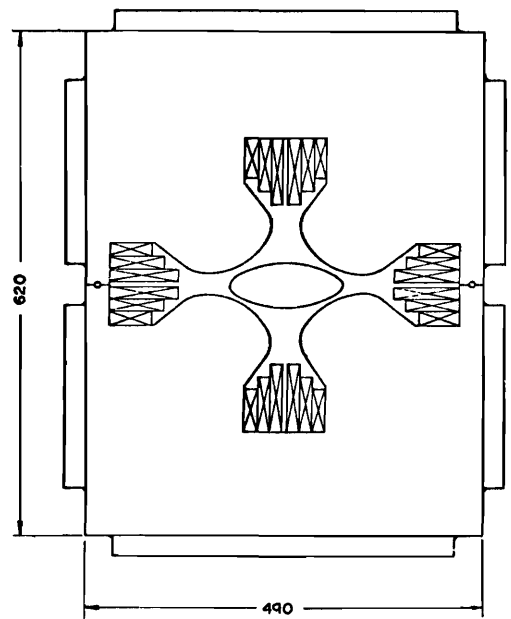


Fig. 32 Cross section of Main ring magnet



$$\text{rot } \vec{H} = \vec{i} \quad \oint_{l+d} \vec{H} \cdot d\vec{l} = \int_S \vec{i} \cdot \vec{n} dS = NI$$

$$H_{\text{iron}} \cdot l + H_{\text{gap}} \cdot d = NI$$

$$\frac{B}{\mu_{\text{iron}}} \cdot l + \frac{B}{\mu_0} \cdot d = NI$$

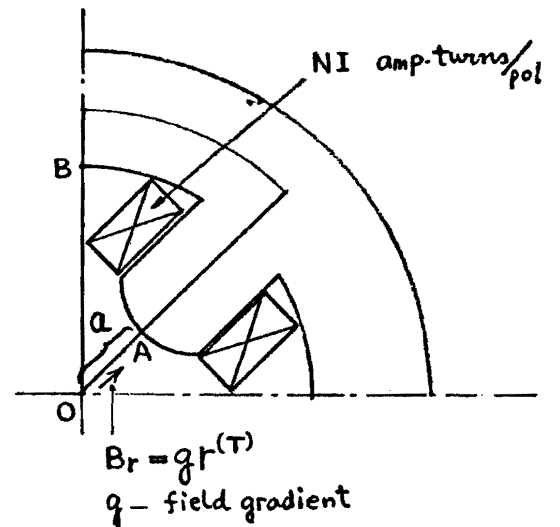
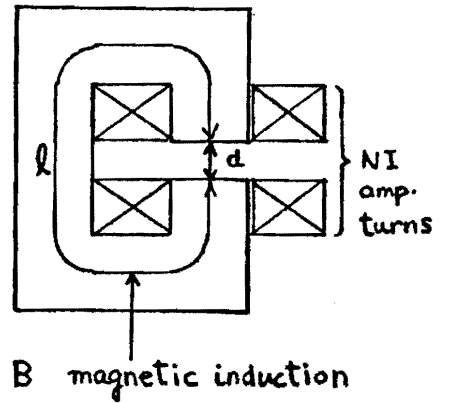
since  $\frac{l}{\mu_{\text{iron}}} \ll \frac{d}{\mu_0} \rightarrow NI \cong \frac{B^{(\tau)}}{\mu_0} \cdot d^{(m)}$   
 $(\mu_0 = 4\pi \times 10^{-7})$

$$\oint \vec{H} \cdot d\vec{l} = \int_{OA} H_r \cdot dr + \int_{AB} \vec{H} \cdot d\vec{l} + \int_{BO} \vec{H} \cdot d\vec{l} = NI$$

$\downarrow$   $\downarrow$   
 $\sim 0$   $\sim 0$   
 (inside iron)  $(\vec{H} \perp d\vec{l})$

$$\int_0^a \frac{1}{\mu_0} q r \, dr \cong NI \rightarrow NI \cong \frac{1}{2} \frac{q}{\mu_0} \cdot a^2$$

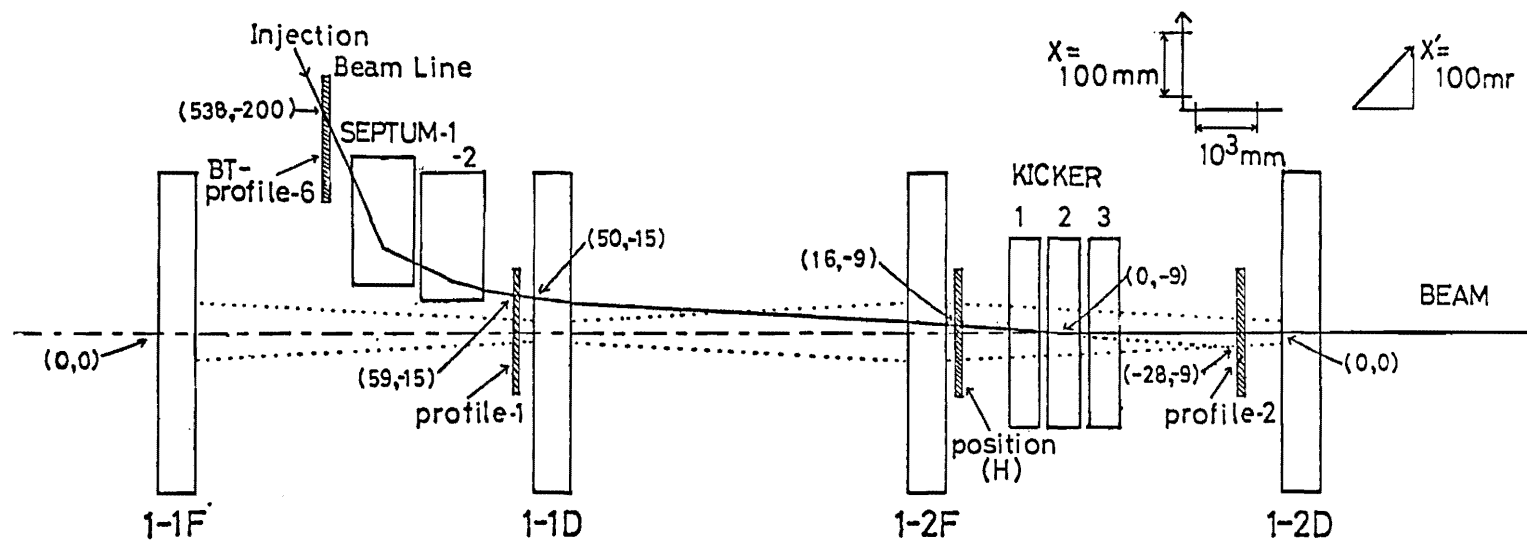
Fig. 33



(2) Injection

The injection of the beam transported from the booster into the main ring is performed with two septum magnets located in the first long straight section ( $L_1$ ) of the first superperiod and four modules of the fast kicker magnet located in the second long straight section ( $L_2$ ) (Fig. 34). The beam with a horizontal position and direction of (+50 mm, -15 mr) with respect to the central axis at the injection point (D quadrupole in  $L_1$ ) crosses the central orbit at the middle of the kickers in  $L_2$  after traversing two quadrupoles and one dipole of the main ring. Then, the kickers, the same type as those used in the booster, bend the beam by about 9 mrad and put it on the central orbit. In this case, both rise and fall time of the kicker pulse fields should be short enough in order that the kick for the injection does not affect beam bunches which have been injected and are circulating in the ring.

BUNCH INJECTION INTO THE MAIN RING

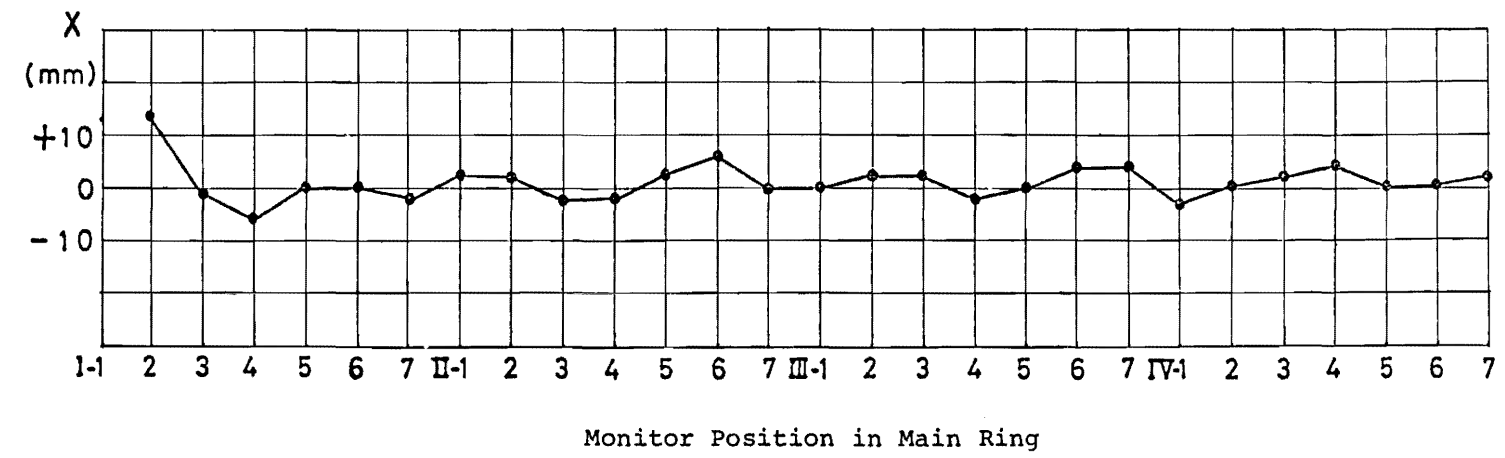


- 163 -

Fig. 34

1-1F & 1-2F: Focusing Quadrupole Magnet  
 1-1D & 1-2D: Defocusing Quadrupole Magnet

COHERENT BETATRON OSCILLATION OF THE FIRST REVOLUTION



### (3) Radio frequency acceleration system

An accelerating field of a constant frequency and amplitude is applied across the accelerating gaps of the main ring during the injection period (~0.5 sec). The accelerating frequency at the injection coincides with that of the booster at the extraction, since the main ring is designed to have the harmonic number of nine and the mean radius of nine times of the booster radius. The acceleration system prepares nine rf buckets in the main ring, which are successively filled up with the beam bunch accelerated in the booster (Fig.35). In this beam transfer scheme (so called synchronized transfer), the bunch injected in the main ring should have such a phase that the bunch is situated at zero synchronous phase of the main ring rf bucket, and such a momentum that the bunch circulates on the central orbit in the ring accurately synchronizing with the rf bucket (Fig.36). Actually, the beam is extracted from the booster at the moment that the beam in the booster is found to have the proper phase and momentum which match with those of the main ring rf bucket. The magnetic field and acceleration system of the booster are so arranged that the beam satisfies such conditions without fail as being accelerated to the top energy of the booster.

The main ring requires a peak accelerating voltage of ~60 kV, and the frequency ranging from 6 MHz (500 MeV) to 8 MHz (12 GeV). We use three accelerating cavities, which are almost same as that used in the booster, to produce required accelerating field. In the case of the main ring, the beam crosses the transition energy at ~6 GeV. The transition energy is approximately given to be [(number of horizontal betatron oscillation per revolution) - 1] × (particle rest energy). At the transition beam loses the phase stability. In the alternating gradient (AG) synchrotron, the stable phase region is the rising side of the voltage across the gap below the transition and is the falling side above the transition. Then, as crossing the transition, the phase of the accelerating field is jumped instantaneously by  $(180^\circ - 2\phi_g)$  with respect to the beam phase (Fig.37).

An error in the mean orbit radius ( $\Delta R$ ) is related to an error in the revolution frequency ( $\Delta f$ ) as  $\frac{\Delta R}{R} = \frac{\gamma^2}{\gamma_{tr}^2 - \gamma^2} \times \frac{\Delta f}{f}$  in AG synchrotron,

where  $\gamma$  is a total energy of the particle divided by its rest energy. This implies that the accelerating frequency must be controlled accurately

BEAM TRANSFER FROM BOOSTER TO MAIN RING

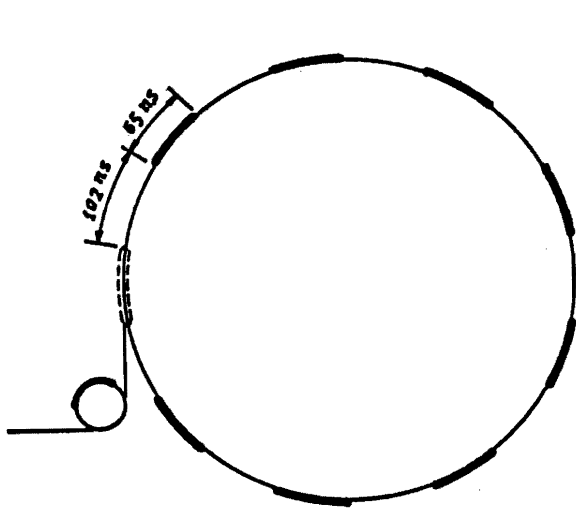


Fig. 35

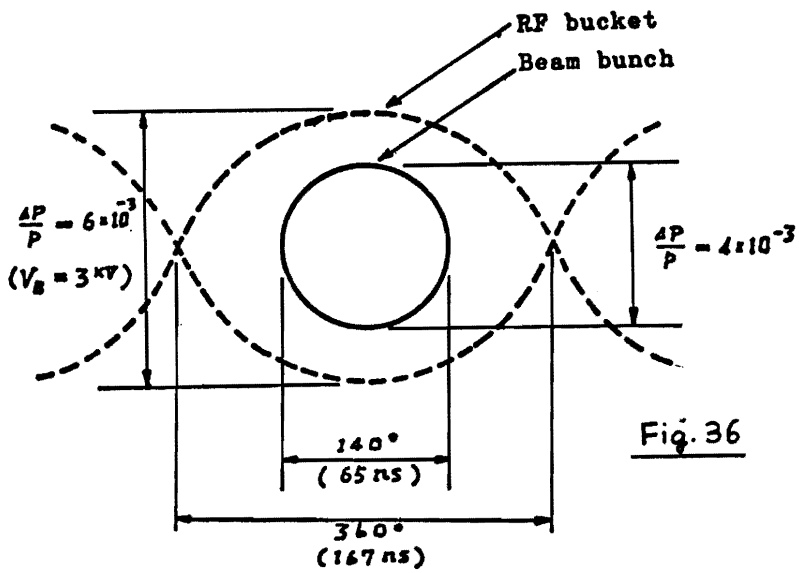
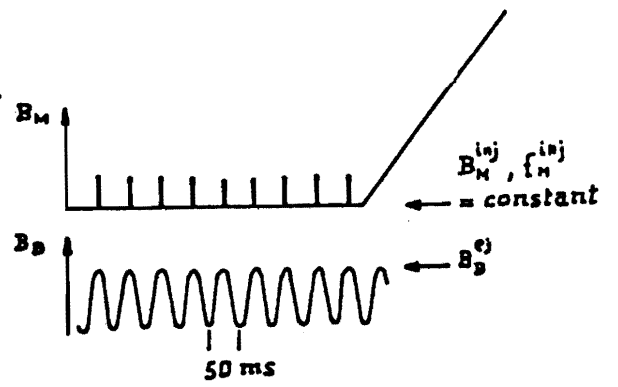


Fig. 36

- Tolerances
- $|P_M - P_B| / P_M < 2 \times 10^{-4}$
  - $|\delta B_M| / B_M < 1 \times 10^{-3}$
  - $|\delta B_B| / B_B < 4 \times 10^{-4}$
  - $|\delta \varphi| < 10^\circ$

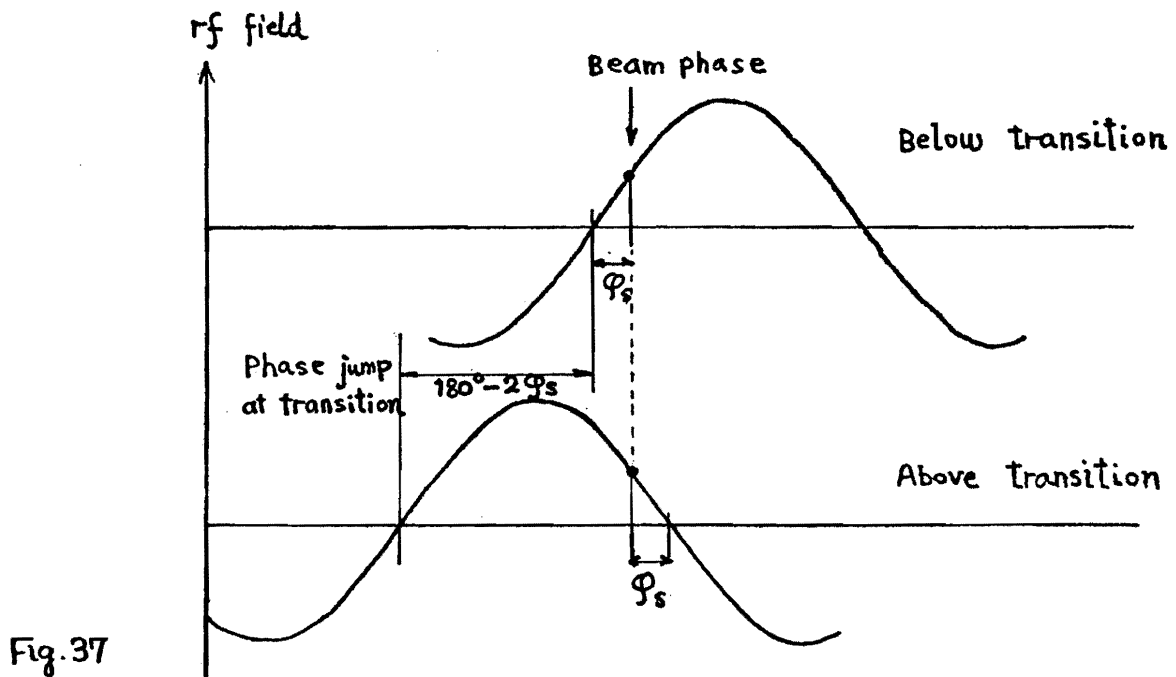
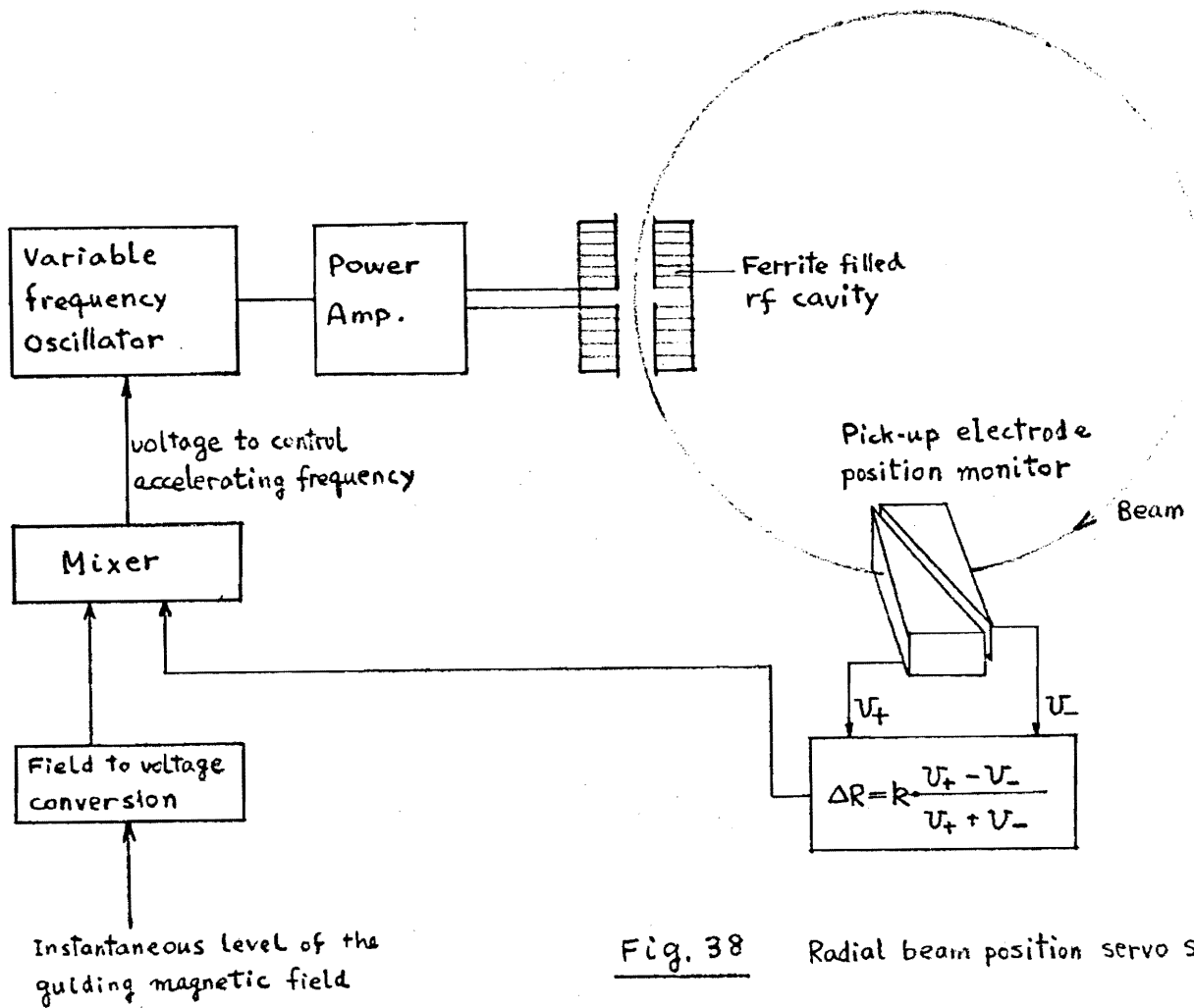


Fig. 37

at around the transition ( $\gamma \sim \gamma_{tr}$ ) so that an increase in the error of the radial motion does not cause a beam loss. The present system is required to generate accelerating frequencies with an accuracy better than  $|\frac{\Delta f}{f}| \lesssim 10^{-6}$ . Such an accurate regulation of the rf frequency is far beyond the stability of the variable frequency oscillator controlled by the magnet field level, and can only be achieved by controlling the oscillator with the radial beam position servo system. Several schemes of the beam controlled frequency system have successfully been applied to the existing synchrotrons. One of them, which is simple in the principle and is actually applied to the present booster rf system, is illustrated in Fig.38. Error signals from the radial pick-up electrode are used to control the master oscillator directly, and correct variations in the radial beam position due to errors in the accelerating frequency.

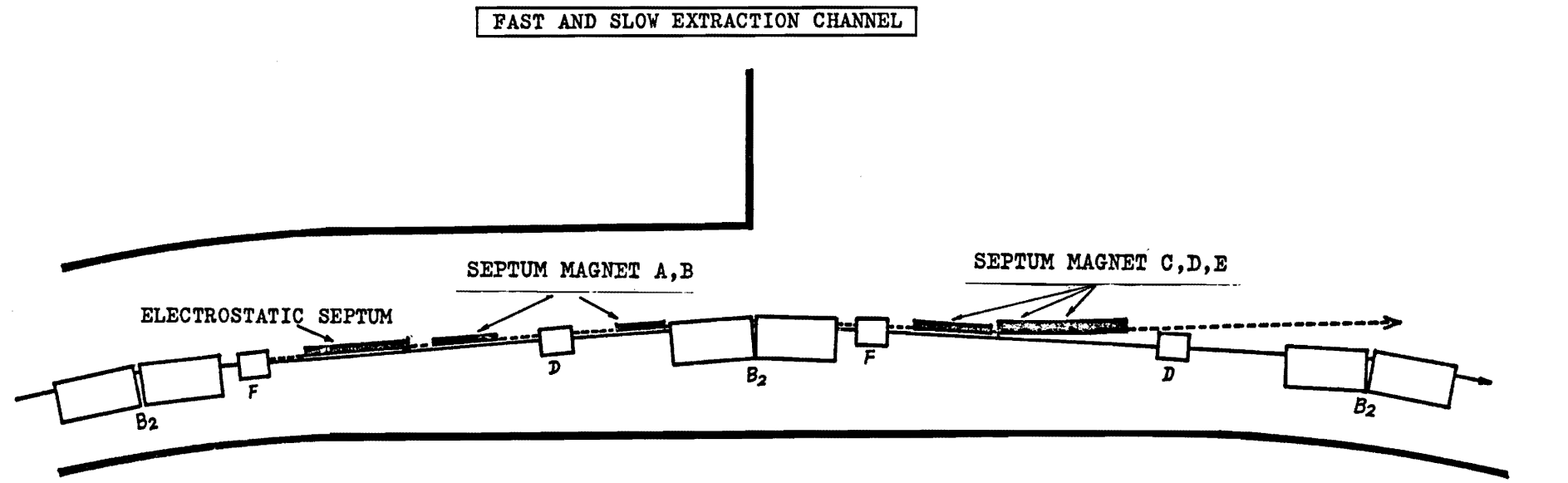


#### (4) Extraction

We have not yet tried the beam extraction from the main ring. Test operations of the fast extraction system are scheduled to start from Dec.1976, and the slow extraction system from ~Oct.1977. First particle physics experiments will start from May 1977 by using secondaries produced at an internal target in the ring. The fast and the slow extraction channel in the ring have structure as illustrated in Fig.39. The essential part of the system is the electrostatic septum inflector. The inflector is shown schematically in Fig.40. The electrode connected to the high electric potential is a titanium plate and faces the wire plane electrode at the ground potential. Thin tungsten wire ( $50 \mu\phi$ ) is wound on a C shaped aluminum frame with a wire spacing of 1.25 mm and winding tension of ~200 g. A special technique to fasten the wire on the frame is developed as illustrated in Fig.41.

A uniform field of about 60 kV/cm is produced in the gap between the titanium electrode and the wire plane leaving a field free region inside the frame. The beam is traversing inside of the wire plane before the extraction, and is split into two parts when the beam is moved across the wire plane at the extraction (Fig.40). One part of the beam which is shaved by the wire plane is deflected by the electric field being separated from the other which traverses the field free side of the wire plane, and is put on the extraction line which includes five units of the septum magnet for the full extraction of the beam from the ring. If a width of the beam shaved out is large enough (~10 mm) compared with the wire diameter ( $50 \mu$ ), a loss of particles due to collisions with the wires can be limited to a tolerable amount.

The fast extraction is performed by sweeping the beam over the wire plane with the fast bump magnets in a period of about six turns of the beam in the ring. On the other hand, in the case of the slow extraction, the beam is slowly spilled into the gap of the electrostatic septum. This is performed by slowly increasing the horizontal width of the beam, the amplitudes of the betatron oscillation, as bringing the oscillation frequency close to that of the half integral resonance ( $\nu_H \cong 7.2 \rightarrow 7.5$ ). The beam is extracted uniformly in the intensity for about 500 msec.



	E.S.	S.M.-A	S.M.-B	S.M.-C	S.M.-D	S.M.-E
SEPTUM THICKNESS(mm)	.05	1	2	13	26	26
LENGTH(m)	.95x3	1	.8	1.4	1.3	1.3
FIELD STRENGTH	60kV/cm	.1T	.2T	1.1T	1.5T	1.5T
DEFLECTION ANGLE(mr)	1.5	2.1	3.3	31	41	43



Fig. 39

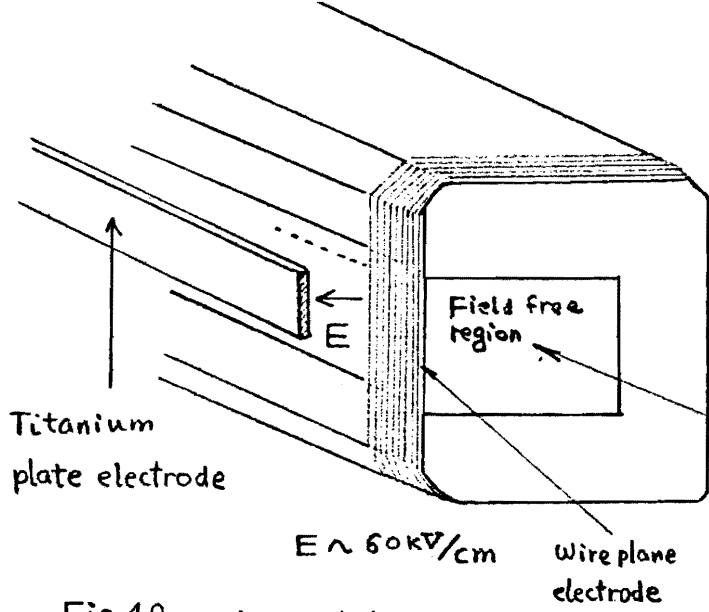


Fig.40 Electrostatic septum

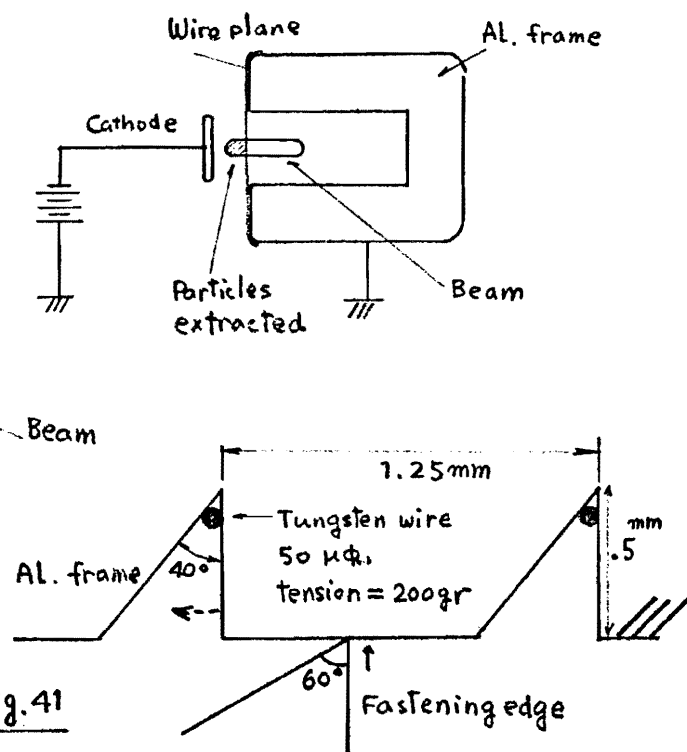


Fig.41

EVOLUTION OF THE BUNCH PHASE RELATIVE TO THE MAIN RING RF PHASE

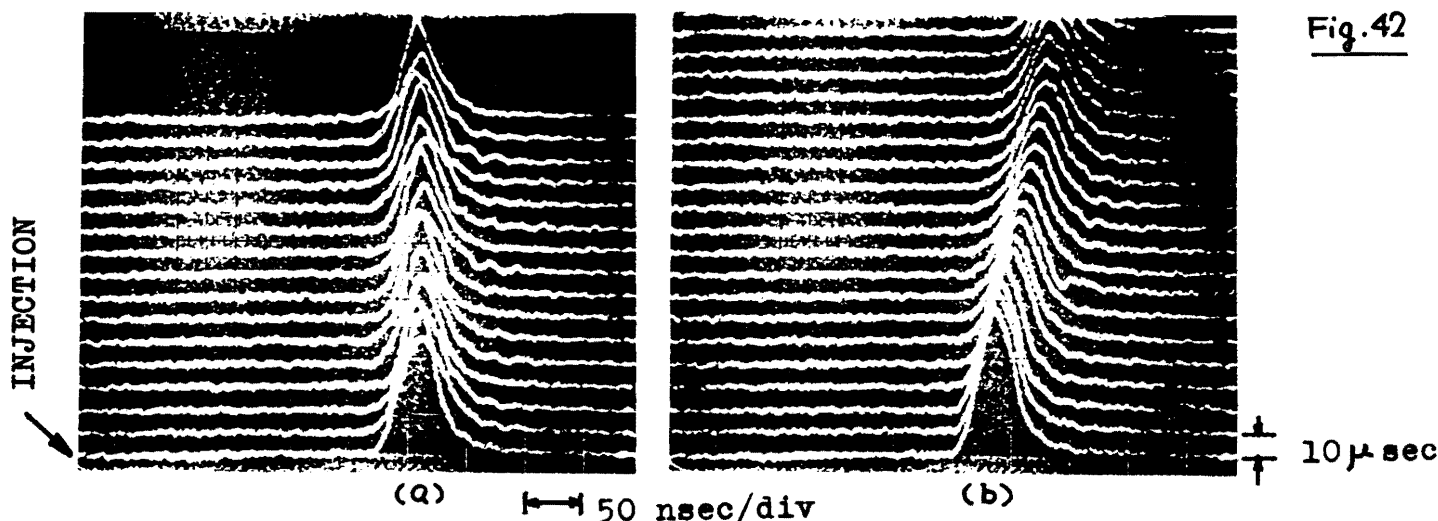


Fig.42

DEBUNCHING OF THE BUNCH IN THE MAIN RING WITHOUT RF ACCELERATION

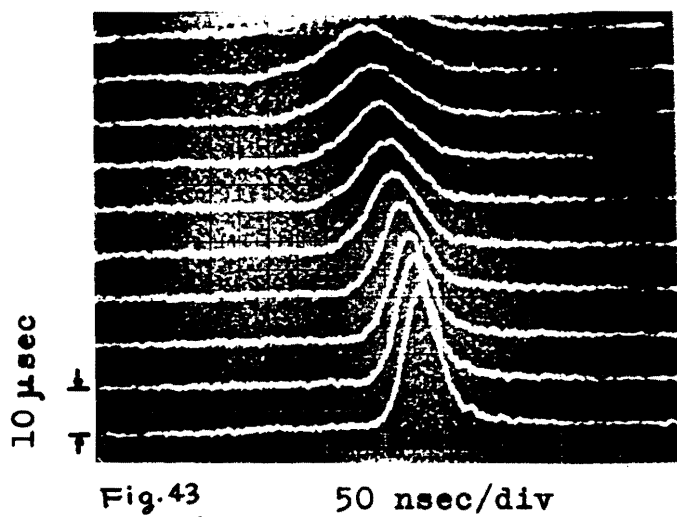


Fig.43

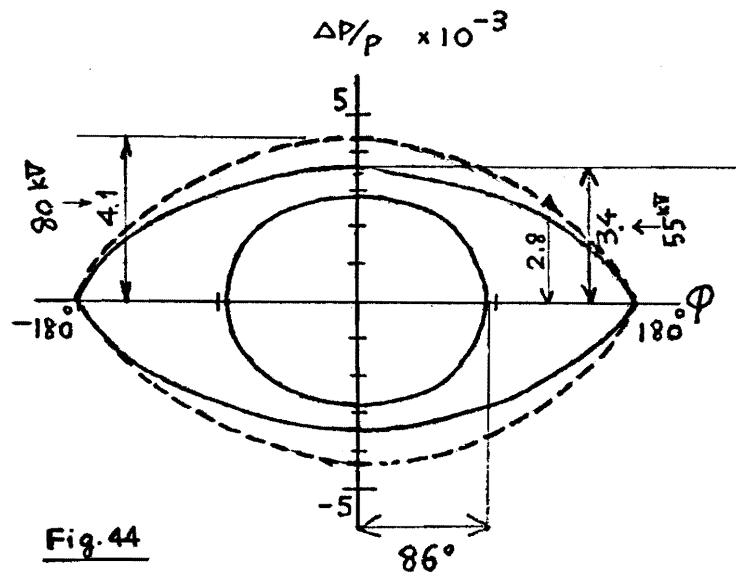


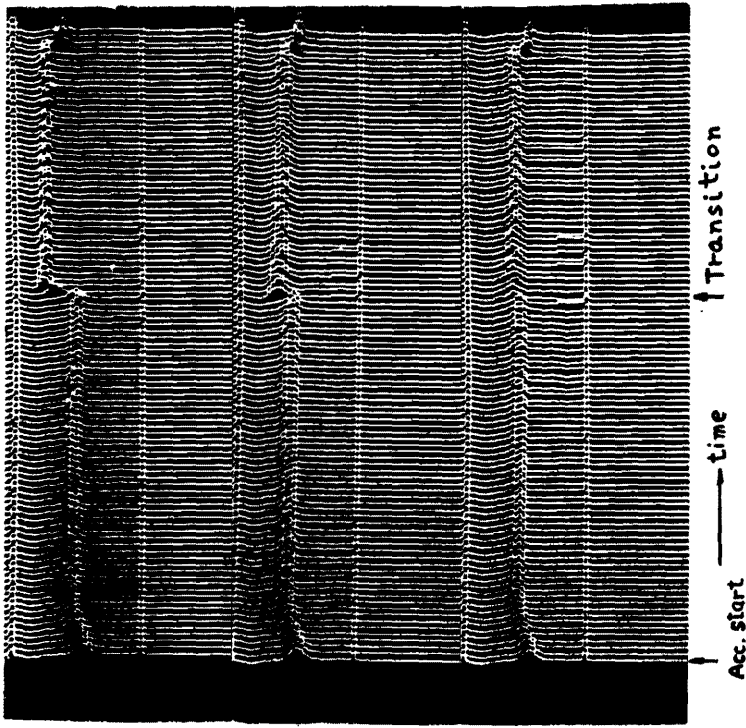
Fig.44

(5) Behaviours of the beam in the main ring

Figure 42 illustrates a longitudinal motion of the beam bunch after the injection. The horizontal sweep of the oscilloscope starts synchronizing with the rf bucket, accordingly Fig.42 (a) shows a case when the synchronized transfer system is operated properly and (b) shows an improper case. Figure 43 is a same type of the photograph as Fig.42 except for that the accelerating rf power is turned off, and shows a free debunching of the beam bunch due to its momentum spread. From the figure, we can estimate the phase and momentum spread of the bunch transferred from the booster (Fig.44).

Evolutions of the horizontal beam profile during the acceleration cycle are shown in Fig.45. We see that the beam suffers considerable perturbations in its radial motion at around the transition. The beam profile is measured by means of the non-destructive profile monitor. The structure of the monitor is illustrated schematically in Fig.46. Two electrodes, one at the ground potential and the other at the high voltage of about 1 kV, are mounted inside the vacuum chamber. A circulating high energy proton liberates ions and electrons by its collision with the residual gas in the vacuum chamber, and ions and electrons are collected on these electrodes. The electrode at the ground potential consists of several of aluminum strips (or thin tungsten wire) which are mounted on the insulated frame. In the radial monitor, the strips lie parallel to the beam direction in a horizontal plane, and a charge collected on a strip gives a measure of number of protons which traverse the same radial position as that of the strip.

Figure 47 shows an example of the beam current in the main ring. In this case, one booster beam pulse is injected at the beginning of the injection period. There are some heavy beam losses after the injection. It has been found that particles with large transverse betatron amplitudes (horizontal or vertical, or both?) are lost during the early stage of the acceleration cycle. To cure the effects, several small multipole magnets will be installed in the ring to correct possible imperfections of the magnetic field. Figure 48 shows a beam current when nine booster pulses are injected successively into the main ring. As seen in the figure, the present status of the main ring is far from the ideal. However, we have just started the detailed studies of the main ring, and the programs to improve the situation are in progress steadily.



Case 1 Case 2 Case 3

Fig. 45 Beam profile in the main ring

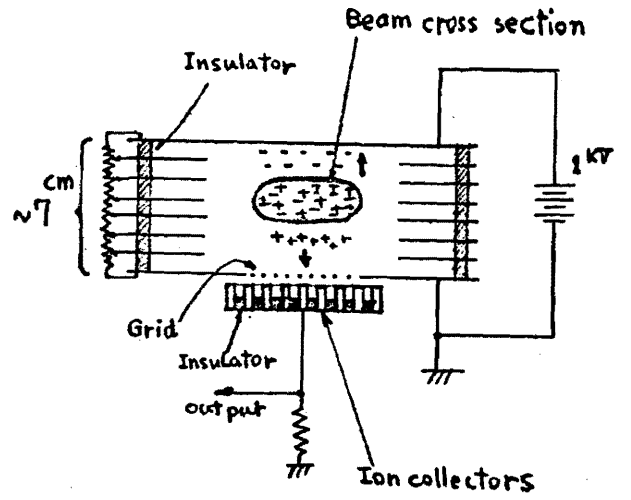


Fig. 46

Non destructive profile monitor

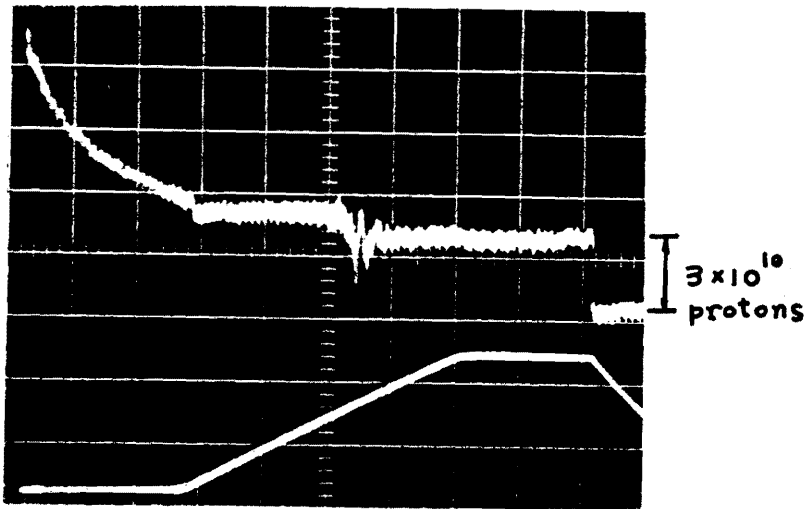


Fig. 46 Beam intensity (Single booster pulse injection)

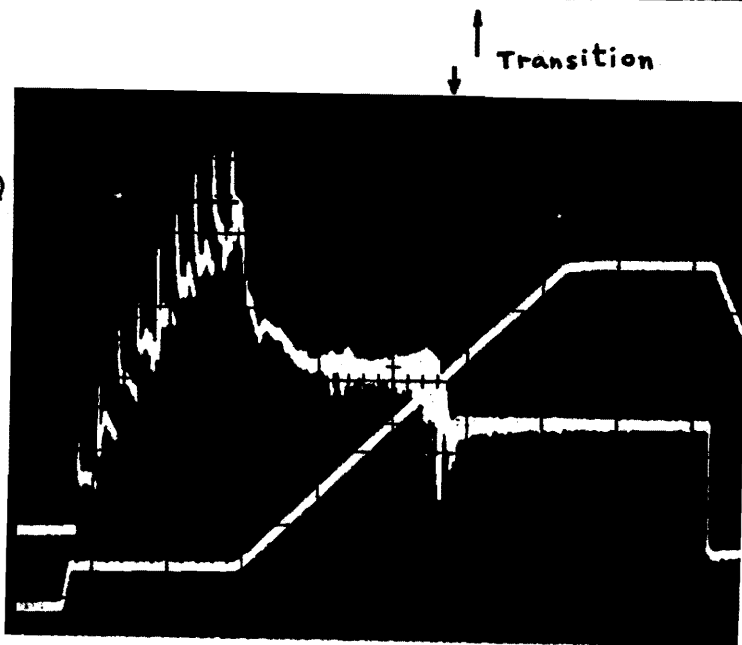


Fig. 47 Beam intensity (Nine booster pulse injection)

$5 \times 10^{11}$  protons

$1.5 \times 10^{11}$  protons

ACKNOWLEDGEMENTS

I would like to thank the members of the KEK accelerator group for valuable discussions and for preparations of the useful materials.